JOURNAL OF GEOPHYSICAL RESEARCH, VOL. 112, F03S07, doi:10.1029/2006JF000559, 2007

Transient channel incision along Bolinas Ridge, California: Evidence for differential rock uplift adjacent to the San Andreas fault

Eric Kirby,[1] Courtney Johnson,[1] Kevin Furlong,[1] and Arjun Heimsath[2]

Received 11 May 2006; revised 24 August 2006; accepted 16 October 2006; published 1 March 2007.

[1] The rates and spatial distribution of active deformation provide critical constraints on the geodynamics of deforming lithosphere, yet such data are often difficult to acquire in eroding landscapes where poor preservation of geomorphic or stratigraphic markers hinders strain reconstruction. Recent advances in understanding of the relationship between bedrock channel profile form and erosion rate have led to their use as an index of rock uplift rate in steady state landscapes. Here we extend this analysis to landscapes experiencing a transient increase in erosion rate using an example from the Marin County region of northern California. We characterize channel and hillslope gradients in a series of small watersheds along a monolithologic portion of the Franciscan terrane in Marin County. Channel steepness indices vary strongly from north to south along the ridge and correspond with the progressive development of relief on threshold hillslopes along valley walls. These patterns argue that recent channel incision has engendered a transient adjustment of hillslope gradient, as incision outpaces soil production rates. These differences in landscape form and inferred incision rate are explained by differential rock uplift within the region east of the San Andreas fault. Relationships between channel gradient and incision rate suggest a threefold to fivefold difference in incision rate across the region and place a minimum bound on differential rock uplift rates. Our study highlights how landscape analysis can place bounds on the distribution of Earth deformation in both space and time and thus lends insight into the processes driving that deformation.

Citation: Kirby, E., C. Johnson, K. Furlong, and A. Heimsath (2007), Transient channel incision along Bolinas Ridge, California: Evidence for differential rock uplift adjacent to the San Andreas fault, *J. Geophys. Res.*, *112*, F03S07, doi:10.1029/2006JF000559.

1. Motivation

[2] Observations of the surface velocity field can provide important constraints on the location, geometry, and slip rates of active faults and thus constitute a foundation for understanding the dynamics of lithospheric deformation; indeed, the advent of high-precision space geodesy over the past two decades has revolutionized the study of active mountain belts. The vertical component of surface deformation, in particular, can place bounds on the geometry and slip rate of thrust fault systems [e.g., *Molnar*, 1987], many of which exhibit blind fault tips that terminate beneath the surface [e.g., *Stein and King*, 1984]. Precise geodetic determination of vertical surface displacements, however, remains a challenging and time-consuming effort, requiring either continuous GPS measurements or traditional leveling surveys [e.g., *Jackson et al.*, 1992]. Moreover, such measurements typically only capture interseismic strain accumulation; long-term rates and patterns remain to be inferred from finite deformation recorded in geologic structures [*Shaw and Suppe*, 1996] or geomorphic markers [*Lavé and Avouac*, 2000].

[3] In the absence of such geologic markers, however, one approach to reconstructing relative differences in the vertical rock velocity field has emerged from the field of tectonic geomorphology. In principle, landscape topography reflects a competition between rock uplift and the rates of erosion [*Howard et al.*, 1994; *Tucker and Slingerland*, 1994], and the sensitivity of geomorphic transport processes to local topographic gradients [see *Dietrich et al.*, 2003] has led to the suggestion that landscape relief in tectonically active regions reflects, to first-order, the rates and patterns of rock uplift [*Whipple et al.*, 1999]. Although a number of studies have focused on broad correlations between erosion rate and topographic relief measured over subwatershed scales (often termed ''local relief'' [see *Hurtrez et al.*, 1999; *Montgomery and Brandon*, 2002]), this measure convolves processes operating in the channel network and on hillslopes. Hillslope gradients approach threshold values as erosion rates begin to outpace the rate of soil production [*Burbank et al.*, 1996] and mass failure by landsliding limits hillslope relief [*Schmidt and Montgomery*, 1995]. Consequently, the utility of hillslope gradients as a metric for erosion rate is restricted to low erosion rate settings. In contrast, the sensitivity the channel network to erosion rate suggests that important information about the rates and patterns of tectonic forcing are present in channel longitu-

[1]Department of Geosciences, Pennsylvania State University, University Park, Pennsylvania, USA.
[2]Department of Earth Science, Dartmouth College, Hanover, New Hampshire, USA.

0148-0227/07/2006JF000559$09.00

dinal profiles [e.g., *Kirby and Whipple*, 2001]. A number of studies provide a theoretical framework for the manner in which channels respond to variations in rock uplift rate [*Howard et al.*, 1994; *Tucker*, 2004; *Whipple and Tucker*, 1999, 2002]; still others present an empirical confirmation of a correlation between channel profile form and erosion rate in field sites where the rates and pattern of tectonic forcing are independently known [*Duvall et al.*, 2004; *Kirby and Whipple*, 2001; *Lague and Davy*, 2003; *Snyder et al.*, 2000]. Together, these studies suggest that bedrock channel profiles provide a powerful means of exploring spatial patterns of differential rock uplift across a landscape [*Kirby et al.*, 2003; *Wobus et al.*, 2003]. Most of these studies were conducted under conditions of steady state erosion, where landscape form is known (or assumed) to be adjusted so that erosion rates everywhere balance rock uplift.

[4] In many landscapes of interest, where deformation rates are not known a priori, this condition is not likely to be met, and thus, if we are to continue to develop our ability to quantitatively extract signals of deformation from landscape topography, we must contend with the transient response of erosional landscapes. Simple models of detachment-limited bedrock channels predict relatively rapid adjustment of local channel gradient to changes in rock uplift rate [*Niemann et al.*, 2001; *Whipple*, 2001], while the diffusive response of slope-dependent soil transport processes leads to longer periods of transient adjustment [e.g., *Fernandes and Dietrich*, 1997; *Roering et al.*, 2001]. Moreover, the potential for feedbacks between hillslope sediment flux and channel incision [*Sklar and Dietrich*, 1998; *Whipple and Tucker*, 2002] and variable lithologic resistance to erosion [e.g., *Anderson et al.*, 2006] may lead to landscape response times that are sufficiently long such that long-term variations in deformation rate ($\sim 10^5$–10^6 yr) associated with the temporal evolution of fault networks [e.g., *Cowie and Roberts*, 2001] may impart morphologically distinct, transient signals to the landscape. In such situations, analysis of landscape topography can help inform tectonic models by providing information on the distribution of deformation in both space and time.

[5] In this contribution, we present an example of such an effort in the coast ranges of Marin County, California (Figure 1). High topography in some portions of the Coast Ranges is associated with active shortening, across restraining bends of the San Andreas [*Anderson*, 1990], or above thrust systems linking right-lateral strike-slip faults in the East Bay [e.g., *Lettis and Unruh*, 2000]. North of San Francisco Bay, however, no active faults are recognized between the San Andreas and the Rogers Creek–Hayward fault system [*Working Group on California Earthquake Probabilities*, 2003], yet the topographic massif of Mount Tamalpais rises to nearly 800 m elevation. Although lithologic heterogeneity within the Franciscan terrane clearly influences the distribution of topography throughout the region [*Blake et al.*, 2000], whether or not the region is undergoing active deformation remains uncertain. To a large degree, the chaotic nature of the bedrock geology precludes traditional efforts to recognize potentially active structures via deformed stratigraphic markers. Here we utilize recent advances in our understanding of the relationship between river longitudinal profiles and rock uplift rates [*Wobus et al.*, 2006b] to test the hypothesis that active, differential rock uplift is, in part, responsible for the high topography in Marin County. Our analysis focuses on the spatial distribution of hillslope and channel gradients across a monolithologic region of the Franciscan terrane, along Bolinas Ridge, adjacent to the San Andreas fault.

2. Background

2.1. Topographic Evolution of the Coast Ranges

[6] Stratigraphic relationships along the western margin of the Central Valley indicate that the central and northern Coast Ranges of California first emerged as a topographic feature in Late Miocene–Early Pliocene time [*Jones et al.*, 2004; *Page et al.*, 1998]. Prior to the Late Miocene, the San Joaquin valley was open to marine circulation [*Bartow*, 1991]; preservation of a Late Neogene shoreline in the eastern Diablo Range [*Graham et al.*, 1984] and a subsequent shift to local sediment sources suggest emergence of this range sometime around ~5 Ma (see discussion by *Jones et al.* [2004]). Although previously interpreted to reflect a increase in the plate convergence at this time [*Page et al.*, 1998], recent determinations of the relative motions of the Pacific and North American plates suggest relatively constant plate motion since at least ~8 Ma [*Atwater and Stock*, 1998], consistent with the present-day velocity field [*Argus and Gordon*, 2001]. Thus, although topography in the vicinity of the Cape Mendicino appears to be a consequence of deformation associated with northward migration of the triple junction [*Furlong et al.*, 2003], the cause of topographic growth of the central Coast Ranges remains somewhat enigmatic, and may be related to changing lithospheric buoyancy beneath the Sierra Nevada [*Jones et al.*, 2004].

[7] Regardless of the ultimate driving forces for topographic growth in the Coast Ranges, present-day topography locally reflects subsequent modification by plate boundary deformation associated with the San Andreas and associated fault systems. Convergence associated with a slight restraining bend in the San Andreas fault system has led to crustal thickening and growth of the Santa Cruz Mountains [*Anderson*, 1990; *Rosenbloom and Anderson*, 1994]. This system appears to have developed as a consequence of progressive linkage and slip transfer as the proto-San Andreas in central California took over from the San Gregorio–Hosgri fault system as the primary structure accommodating transcurrent shear [*Furlong and Schwartz*, 2004]. In an analogous setting, recent work in the East Bay region [*Lettis and Unruh*, 2000] suggests that shortening associated with slip transfer across restraining steps in East Bay fault systems may be accommodated on blind fault systems responsible for relative topographic highs at the fault terminations (e.g., East Bay Hills, Mount Diablo).

[8] North of San Francisco, the topography of the Coast Ranges in Marin County is subdued relative to the ranges north and south (Figure 1). In general, mean elevations climb gently toward the south, reaching a maximum at Mount Tamalpais, immediately north of the Marin Headlands (Figure 1). Marin County is underlain by the Franciscan complex, a complicated mix of rock types ranging from mélange and serpentinite to lithic-rich wackes [*Blake et al.*, 2000]. The consequent variations in rock strength across the region appear to influence landscape form; there

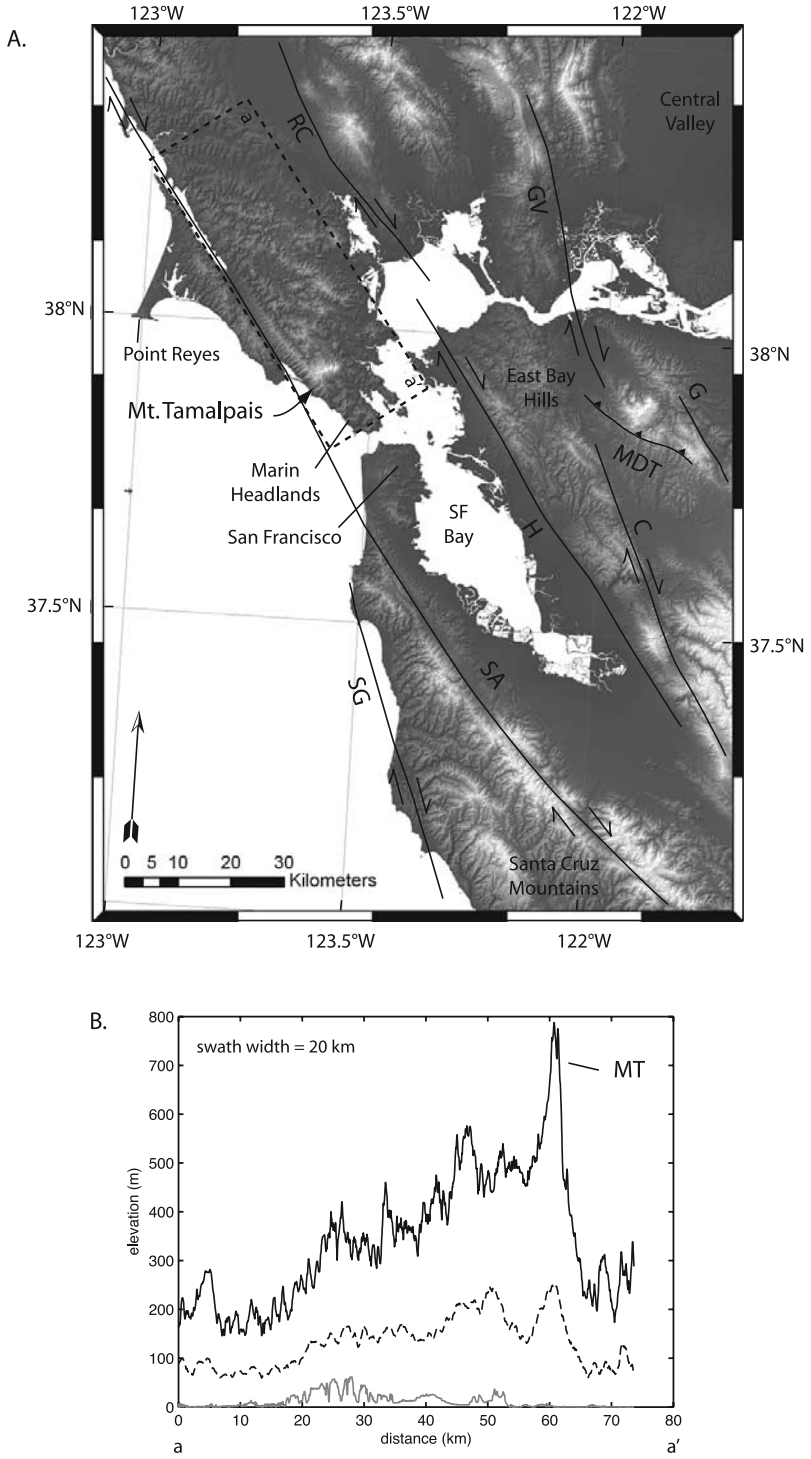

Figure 1. (a) Location map of the study area showing topography, physiographic features, and major active faults in the San Francisco Bay region. Abbreviations are as follows: C, Calaveras fault; GV, Green Valley fault; G, Greenville fault; H, Hayward fault; MDT, Mount Diablo thrust; RG, Rogers Creek fault; SA, San Andreas fault; SG, San Gregorio fault. (b) Swath profile of topography (a-a′) showing broad increase in topographic relief from northwest to southeast in Marin County. Maximum (solid line), minimum (shaded line), and mean (dashed line) elevations extracted from a 20 km wide swath (location is shown as dashed box in Figure 1a). Data source is USGS National Elevation Dataset.

is a strong correspondence between mapped lithologies and topographic highs throughout the Marin County region [*Blake et al.*, 2000]. This interpretation has typically extended to the massif of Mount Tamalpais (Figure 2). Interestingly, however, the massif itself is underlain by the same rock type as the northern part of the Marin Peninsula (Figure 2), and the abrupt difference in relief across the southern flank of Mount Tamalpais (Figure 1b) is not

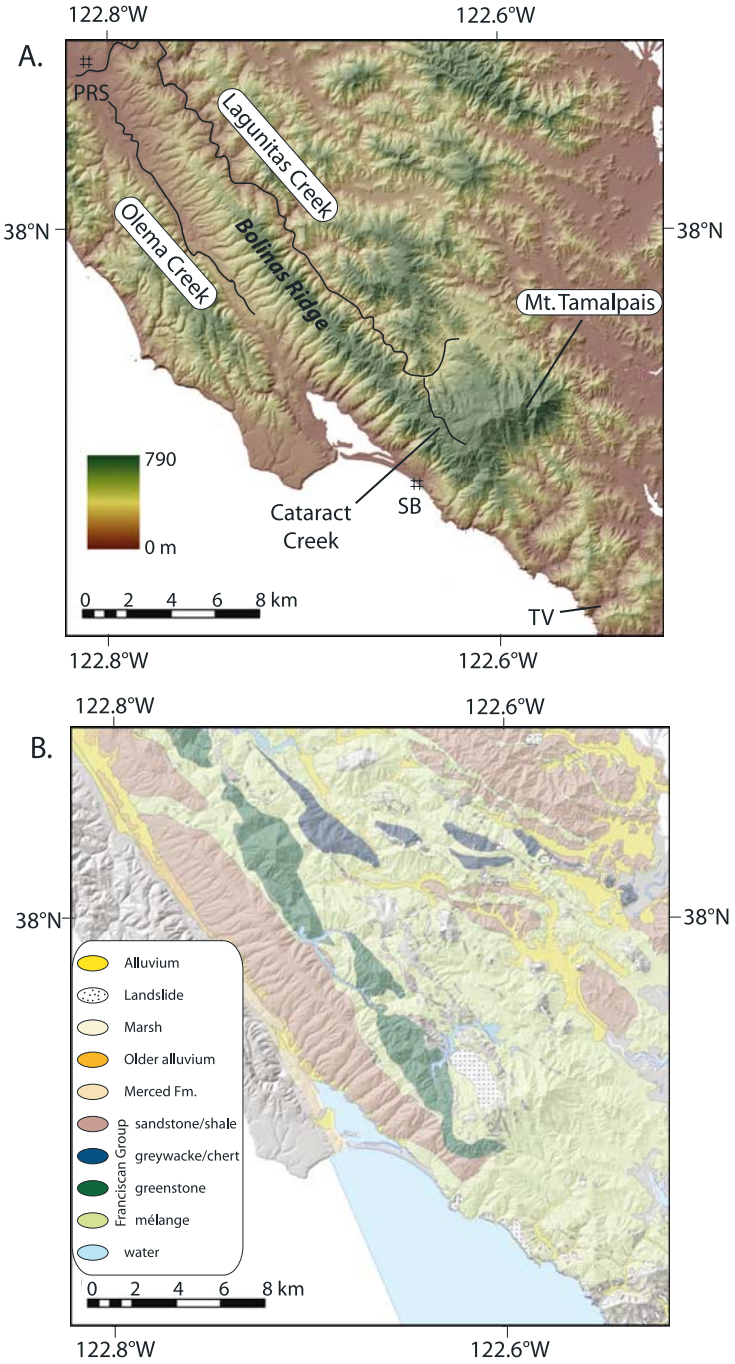

Figure 2. (a) Color-shaded relief map of topography of the Marin County–Mount Tamalpais region showing physiographic features of the study area. TV, Tennessee Valley; PRS, Point Reyes Station; SB, Stinson Beach. (b) Geologic map simplified from *Blake et al.* [2000]. Note the uniform Franciscan sandstone underlying Bolinas Ridge.

obviously a consequence of variable lithologic resistance to erosion.

[9] The landscapes of coastal California, and the Marin County region in particular, have motivated the development of a significant body of work on the rates and processes of soil production and transport on hillslopes [*Dietrich et al.*, 1992, 1993; *Heimsath et al.*, 1997, 1999, 2005; *Montgomery and Dietrich*, 1988, 1989, 1992, 1994]. Of particular relevance to our study is the demonstration that soil depth, soil production rate (as measured by concentrations of ^{10}Be and ^{26}Al in bedrock at the base of the soil), and topographic curvature are highly correlated on small, divergent ridge crests and noses in this landscape [*Heimsath et al.*, 1997, 1999, 2005], an observation that led these authors to conclude that soil production rate declines exponentially with increasing soil thickness. Moreover, these studies found remarkably similar rates of soil production in two separate sites, one in the Marin Headlands [*Heimsath et al.*, 1997, 1999] underlain by greywacke and one on Point Reyes Peninsula [*Heimsath et al.*, 2005],

underlain by Salinian granite. Taken together, these studies suggest similar rates of ridge crest lowering (0.06–0.1 mm/yr) throughout portions the Marin County region, irrespective of bedrock lithology.

2.2. Channel Profile Response to Rock Uplift

[10] The sensitivity of fluvial channels to tectonic forcing has engendered a suite of studies investigating the theoretical parameterization of the processes of channel incision into bedrock [*Hancock et al.*, 1998; *Howard*, 1994; *Howard et al.*, 1994; *Sklar and Dietrich*, 1998, 2004; *Whipple et al.*, 2000; *Willgoose et al.*, 1991], the response of such models to variations in tectonic and climatic forcing [*Tucker*, 2004; *Whipple and Tucker*, 1999, 2002], and empirical testing of models in regions of known tectonic forcing [*Duvall et al.*, 2004; *Kirby and Whipple*, 2001; *Lague and Davy*, 2003; *Snyder et al.*, 2000; *Tomkin et al.*, 2003; *van der Beek and Bishop*, 2003]. We intentionally focus our discussion here on empirical evidence for a correlation between channel gradients and fluvial incision rates, and present only a rudimentary consideration of channel incision models in the context of unresolved issues. For a detailed discussion of bedrock incision models, the reader is referred to a recent review by *Whipple* [2004]. We wish to exploit the manner in which channels respond to tectonic forcing to test hypotheses for active deformation within the Marin County/Mount Tamalpais region. In this section, we briefly review the theoretical and empirical basis for understanding the response of fluvial channels to variations in rock uplift.

[11] Across a wide variety of tectonic and climatic settings, topography of fluvial channels typically exhibits a scaling between local channel gradient (S) and the contributing drainage area (A) upstream [*Flint*, 1974; *Hack*, 1973; *Howard and Kerby*, 1983]:

$$S = k_s A^{-\theta} \tag{1}$$

where S is the local channel gradient, A represents upstream drainage area, and k_s and θ are the steepness and concavity indices, respectively. Note that this scaling only holds for drainage areas above a critical threshold (A_{cr}) [e.g., *Tarboton et al.*, 1989]. The break in scaling from a region where gradients are invariant with increasing drainage area, to one where gradients decrease systematically with increasing area, is thought to represent either a transition from hillslopes to channels [*Montgomery and Foufoula-Georgiou*, 1993], or perhaps a transition from debris flow to fluvial processes [*Lague and Davy*, 2003; *Stock and Dietrich*, 2003]. Numerous simple models for fluvial incision into bedrock (both detachment-limited and transport-limited models) predict power law relations between channel gradient and drainage area of the form of equation (1) [*Howard et al.*, 1994; *Whipple and Tucker*, 1999, 2002; *Willgoose et al.*, 1991]. Moreover, steady state realizations of these models (defined as the condition where erosion rate balances rock uplift everywhere along the channel profile) make two key predictions: (1) that the concavity index (θ) is independent of rock uplift rate (U), provided U does not vary along the channel length [e.g., *Kirby and Whipple*, 2001] and (2) that there is a positive, monotonic correlation between the steepness index (k_s) and rock uplift rate. Essentially, steeper channels are more effective at eroding the channel bed (for a given discharge); thus, as rock uplift rates increase, so should channel gradients.

[12] There are a number of factors not incorporated into these models that may be expected to impact the quantitative relation between k_s and U. These include (1) nonlinearities in the incision process [*Whipple and Tucker*, 1999], including thresholds for incision [*Snyder et al.*, 2003; *Tucker*, 2004; *Tucker and Bras*, 2000], (2) adjustments in channel width and sinuosity [*Duvall et al.*, 2004; *Finnegan et al.*, 2005; *Lavé and Avouac*, 2000], (3) adjustments in hydraulic roughness, grain size of bed material, and/or extent of alluvial cover [*Sklar and Dietrich*, 1998, 2001, 2004], (4) changes in the efficacy of erosive debris flows [*Stock and Dietrich*, 2003], and (5) orographic enhancement of precipitation [*Roe et al.*, 2002, 2003]. Moreover, rock mass quality and strength profoundly influences k_s [*Duvall et al.*, 2004; *Kobor and Roering*, 2004; *Moglen and Bras*, 1995; *Stock and Montgomery*, 1999] and one needs to be cautious when deconvolving the effects of lithologic variability from uplift rate signals.

[13] Despite these uncertainties, strong empirical support for a positive functional relationship between channel steepness indices and rock uplift rate is emerging from landscapes across the globe [*Wobus et al.*, 2006b]. Results from studies conducted in coastal California and in the foothill ranges of the Nepalese Himalaya place bounds on the functional relationship between channel gradients and rock uplift rate. *Snyder et al.* [2000, 2003] and *Duvall et al.* [2004] both compared small, coastal channels experiencing variable rock uplift rate, but with minimal variations in lithology and climate within each study area. In both field sites, the functional relationship between channel steepness and erosion rate appeared to be nonlinear, such that differences in k_s were more subdued than differences in erosion rate. This effect was interpreted to reflect incision thresholds in the King Range [*Snyder et al.*, 2000, 2003] and systematic changes in channel width in the western Transverse Ranges [*Duvall et al.*, 2004]. In contrast, studies the Siwalik Hills of central Nepal [*Kirby and Whipple*, 2001] demonstrated that systematic changes in channel gradient were linearly correlated with variable rock uplift rate across a fault bend fold [cf. *Wobus et al.*, 2006b]. In a comparative study of colluvial and/or debris flow channels in the same landscape, *Lague and Davy* [2003] also documented a linear relationship between channel gradient and rock uplift rate.

[14] Relatively few attempts have been made to invert this approach and utilize spatial distributions of channel gradient to place bounds on variations of rock uplift across a landscape [*Hodges et al.*, 2004; *Kirby et al.*, 2003; *Wobus et al.*, 2003]. Typically, these studies are forced to contend with the possibility that channel profiles are in a transient state of response, either to climatic or tectonic changes in boundary conditions. Geometric analyses suggest that, if the fluvial system responds to changes in boundary conditions as a kinematic wave [*Niemann et al.*, 2001; *Whipple*, 2001], the transient response may be straightforward, characterized by a relatively constant vertical knickpoint velocity. However, where thresholds in sediment flux and transport stage play an important role [e.g., *Sklar and Dietrich*, 2004], the transient response may be more complex, characterized by a diffusive change in channel gradient [*Whipple and Tucker*, 2002] or oversteepening of channel reaches below knick-

points [*Crosby and Whipple*, 2006] or above tributary junctions [*Wobus et al.*, 2006a].

[15] In summary, although quantitative mapping of channel gradients into erosion rate remains an elusive goal, analysis of channel profiles can provide first-order insight into the relative patterns of rock uplift across a landscape [*Wobus et al.*, 2006b]. In particular, when coupled with additional measures of erosion rates (e.g., cosmogenic isotopes and/or thermochronologic methods), such analysis can place important bounds on the distribution of deformation within a landscape.

3. Field Site

[16] As noted above, the heterogeneous geology of the Franciscan terrane renders traditional methods of recognizing active deformation in Marin County difficult. Moreover, variations in lithology can exert a strong control on landscape relief and channel profile form [*Moglen and Bras*, 1995]. In this contribution, we focus on the geomorphic development of Bolinas Ridge, a ~25 km long, linear ridge, adjacent and parallel to the San Andreas fault (Figure 2). The ridgeline climbs from low elevations near ~200 m at its northern end, near the town of Olema to elevations exceeding ~600 m along the western flank of Mount Tamalpais, mimicking the broad overall increase in elevations across Marin County (Figure 1b). Numerous short, steep channels are developed along the western flank of the ridge, many of which have carved deep canyons. Importantly, the ridge is underlain along nearly its entire length by a large, contiguous lens of Cretaceous sandstone within the Franciscan complex [*Blake et al.*, 2000] (Figure 2), allowing comparison of channel profile form in the absence of lithologic differences observed elsewhere in Marin County. Moreover, precipitation in the Mediterranean climate of the region occurs primarily during major winter storms, and, in the absence of blocking topography between the ridge and the Pacific Ocean, we expect that climatic variations are minimal along this short coastal transect. Thus comparison of channels from north to south along the flanks of the ridge provides a framework for assessing potential variations in rock uplift rate along a transect parallel to the San Andreas fault. Our analysis relies primarily on analysis of channel and hillslope profiles extracted from a digital elevation model (DEM), but is guided by field observations along select channels.

3.1. Stream Profile Analysis

[17] We examined 40 channels draining the western flank of Bolinas Ridge, each with similar channel lengths and catchment areas that allow a straightforward comparison of watershed characteristics along the length of the ridge (Table 1). We also examined channels within the Cataract/Lagunitas creek watershed, east of the ridge crest. We extracted channel profiles from a digital elevation model (USGS NED data, 10 m nominal resolution). We utilize flow routing and watershed definition algorithms standard in the GIS package ArcInfo. Channel profiles are extracted and analyzed following methods developed by *Snyder et al.* [2000] and *Kirby et al.* [2003]. We removed spikes along the channel profile and smoothed the data using a moving average of 30 pixels. This window size was chosen to filter high-frequency noise associated with the digital data, while still retaining the overall form of the profile. Channel gradients were calculated over a fixed vertical interval of 10 m. For a complete description of data processing and analytical techniques, the reader is referred to a recent review by *Wobus et al.* [2006b].

[18] Regression of local channel gradient versus upstream drainage area yielded estimates of the steepness and concavity indices (k_s and θ, respectively). Regressions were limited to the portion of the data that visually exhibited a scaling between channel gradient and drainage area; this is referred to herein as the fluvial portion of the channel network, although we note that many of these channels likely convey debris flows periodically. Hillslopes were excluded from the regressions, as were depositional fan aprons at the mouths of some of the channels (Figure 2). The upstream bound on the regression interval was chosen at the transition from a region of quasi-invariant gradient (inferred to represent hillslopes and/or colluvial channels) to one where gradients decrease with increasing drainage area (see examples in Figure 3). We acknowledge that in many cases, this transition may occur over a range of drainage area, and we recognize that the relatively coarse resolution of the DEM may mask a possible topographic expression of the transition from debris flow to fluvial processes [e.g., *Stock and Dietrich*, 2003]. We are interested, however, in the first-order differences in channel form along strike of the ridge, and for these purposes, small differences in the upstream bound of the regression do not significantly influence the results (Table 1). In most cases, we observe smooth, concave-up profiles, but where channels exhibited distinct knickpoints separating reaches of varying gradient (discussed below), we regressed each reach independently.

[19] In principle, the steepness index (k_s) provides a direct measure of channel steepness that is readily obtained by regression of gradient-drainage area data [*Howard*, 1994; *Willgoose*, 1994]. However, because of the inherent correlation between regression intercept (k_s) and regression slope (θ), direct comparisons among channels of different size and/or concavity can be difficult with this method [*Wobus et al.*, 2006b]. Here we utilize two methods to normalize channel gradients. The first of these, the reference slope method, was proposed by *Sklar and Dietrich* [1998] and is defined as that channel gradient (S_r) measured from equation (1) at a reference drainage area (A_r). This method overcomes the dependence of regression intercept on regression slope, but is most appropriate at or near the midpoint of regression intervals, thus preventing comparison of channels of widely varying size. A second method, referred to as a normalized steepness index [*Wobus et al.*, 2006b], calculates a normalized steepness index (k_{sn}) for a reference value of channel concavity (θ_{ref}). In practice, θ_{ref} is typically chosen as the mean of observed θ values in undisturbed channel segments in a given study area. In principle, however, relative differences in k_{sn} do not depend on the choice of θ_{ref} [*Wobus et al.*, 2006b]. In this study, we choose a value for θ_{ref} of 0.45, that allows for ready comparison to previous studies [e.g., *Duvall et al.*, 2004; *Snyder et al.*, 2003; *Wobus et al.*, 2006b].

[20] Our analysis reveals pronounced systematic variations in channel gradient along the western flank of Bolinas Ridge and within the Lagunitas Creek watershed (Figures 3

Table 1. Topographic Characteristic of Channel Profiles Along Bolinas Ridge[a]

Channel[b]	Distance,[c] km	A_{min}, m^2	A_{max}, m^2	θ	k_s	k_{sn}[d]	k_{sn}[e]	S_r	Name
1	1.9	4.29E + 04	9.19E + 05	0.58	1.08E + 02	19.1	18.4 – 19.9	0.051	
2	2.4	1.79E + 04	9.95E + 05	0.49	2.83E + 01	16.7	16.4 – 17.0	0.044	
3	2.8	3.25E + 04	9.95E + 05	0.51	3.96E + 01	17.9	17.5 – 18.2	0.047	
4	3.1	2.46E + 04	9.56E + 05	0.60	1.13E + 02	17.4	16.7 – 18.1	0.043	
5	3.3	1.86E + 04	9.56E + 05	0.48	2.42E + 01	17.6	17.1 – 18.2	0.046	
6	4.6	1.86E + 04	1.54E + 06	0.40	9.51E + 00	16.8	16.2 – 17.4	0.049	
7	5.5	4.47E + 04	1.04E + 06	0.71	5.47E + 02	20.5	19.3 – 21.7	0.048	
8	5.9	3.97E + 04	6.68E + 05	1.13	8.83E + 04	15.3	13.6 – 17.0	0.032	
9	6.1	3.00E + 04	6.96E + 05	0.59	1.03E + 02	15.9	15.2 – 16.6	0.043	
10	6.8	5.82E + 04	5.37E + 05	0.95	9.21E + 03	20.1	17.4 – 22.9	0.036	
10	*6.8*	*5.72E + 05*	*2.42E + 07*	*0.20*	*8.68E – 01*	*26.8*	*25.5 – 28.2*	*0.066*	
11	7.0	2.56E + 04	4.86E + 05	0.58	9.02E + 01	19.5	18.2 – 20.8	0.045	
11	*7.0*	*1.06E + 06*	*2.31E + 07*	*0.13*	*4.87E – 01*	*43.3*	*41.9 – 44.6*	*0.088*	
12	7.2	6.92E + 04	6.96E + 05	0.98	1.27E + 04	16.9	15.2 – 18.5	0.032	
12	*7.2*	*1.06E + 06*	*2.31E + 07*	*0.13*	*4.87E – 01*	*43.3*	*41.9 – 44.6*	*0.088*	
13	7.6	5.24E + 04	3.27E + 05	1.05	1.77E + 04	15.1	13.6 – 16.7	0.020	
13	*7.6*	*3.02E + 05*	*5.26E + 05*	*−1.90*	*2.30E – 12*	*31.4*	*28.3 – 34.5*	*0.155*	
14	7.9	4.84E + 04	5.06E + 05	0.79	1.36E + 03	21.9	20.2 – 23.6	0.045	
14	*7.9*	*5.26E + 05*	*1.04E + 06*	*0.04*	*1.37E – 01*	*36.0*	*34.1 – 37.8*	*0.079*	
15	9.2	6.14E + 04	1.12E + 06	0.38	1.09E + 01	26.7	26.0 – 27.4	0.079	
16	9.8	1.16E + 05	1.74E + 06	0.49	6.99E + 01	39.0	38.4 – 39.6	0.107	
17	10.7	2.03E + 05	1.31E + 06	1.00	5.78E + 04	33.9	32.0 – 35.8	0.110	
18	11.7	3.52E + 04	1.37E + 06	0.60	2.56E + 02	35.7	34.5 – 36.9	0.092	
19	11.9	2.11E + 05	1.17E + 06	1.47	2.02E + 07	35.4	31.9 – 38.9	0.083	
20	12.1	1.21E + 05	9.95E + 05	1.03	5.35E + 04	32.4	28.7 – 36.1	0.076	
21	12.7	1.21E + 05	5.70E + 05	1.14	1.97E + 05	37.3	34.9 – 39.6	0.067	
22	13.1	1.66E + 05	7.53E + 05	1.16	2.91E + 05	29.8	27.3 – 32.2	0.069	
23	13.4	9.90E + 04	9.95E + 05	0.83	4.85E + 03	32.6	31.1 – 34.1	0.089	
24	14.0	8.64E + 04	4.19E + 05	0.97	1.98E + 04	34.0	32.0 – 35.9	0.056	
24	*14.0*	*4.40E + 05*	*6.61E + 05*	*−0.27*	*4.92E – 03*	*72.9*	*70.7 – 75.1*	*0.172*	
25	14.4	1.12E + 05	1.67E + 06	0.58	2.59E + 02	52.1	51.4 – 52.8	0.128	
26	15.2	5.22E + 04	1.12E + 06	0.58	2.05E + 02	42.4	41.3 – 43.5	0.104	
26	*15.2*	*1.14E + 06*	*1.40E + 06*	*−0.78*	*2.00E – 06*	*74.3*	*70.8 – 77.9*	*0.056*	
27	15.9	6.92E + 04	1.21E + 06	0.58	2.71E + 02	49.2	48.6 – 49.9	0.132	Copper Mine Gulch
28	16.5	4.20E + 04	1.03E + 06	0.35	1.33E + 01	49.1	48.1 – 50.1	0.135	
29	16.9	2.21E + 04	1.48E + 06	0.42	3.87E + 01	53.9	53.3 – 54.5	0.148	Wilkins Gulch
30	17.6	5.97E + 04	8.21E + 05	0.51	1.32E + 02	68.7	67.4 – 70.1	0.175	Pike County Gulch
30	*17.6*	*8.23E + 05*	*1.47E + 06*	*0.22*	*2.85E + 00*	*76.7*	*75.9 – 77.4*	*0.167*	
31	18.4	1.14E + 05	5.77E + 05	0.38	2.12E + 01	53.0	52.8 – 53.3	0.153	
31	*18.4*	*5.81E + 05*	*7.90E + 05*	*1.03*	*1.88E + 05*	*86.5*	*84.7 – 88.3*	*0.267*	
32	18.8	6.27E + 04	7.04E + 05	0.50	9.96E + 01	51.5	50.3 – 52.7	0.134	Audubon Canyon
32	*18.8*	*7.16E + 05*	*1.04E + 06*	*0.54*	*3.05E + 02*	*93.7*	*91.9 – 95.4*	*0.256*	
33	19.7	7.20E + 04	1.37E + 06	0.34	1.83E + 01	72.6	71.6 – 73.6	0.203	
34	20.4	1.16E + 05	1.48E + 06	0.23	3.83E + 00	72.1	71.1 – 73.2	0.192	Morses Gulch
35	21.1	2.68E + 05	1.60E + 06	0.63	8.65E + 02	78.4	77.5 – 79.3	0.231	McKinnan Gulch
36	22.3	3.54E + 05	1.48E + 06	0.83	2.36E + 04	126.2	122.6 – 129.8	0.417	Stinson Gulch
37	23.7	3.14E + 05	1.16E + 06	0.10	1.06E + 00	116.2	114.2 – 118.3	0.301	
38	25.7	1.89E + 05	1.21E + 06	0.84	8.27E + 03	44.3	41.9 – 46.7	0.133	Steep Ravine Canyon
38	*25.7*	*1.22E + 06*	*2.82E + 06*	*1.36*	*3.64E + 07*	*76.6*	*73.3 – 79.9*	*0.681*	
39	26.6	7.20E + 04	2.04E + 06	0.21	2.26E + 00	57.5	55.6 – 57.5	0.153	Lone Tree Creek
40	27.6	1.65E + 04	1.04E + 06	0.38	1.90E + 01	46.5	45.6 – 47.5	0.133	Cold Stream
c		4.22E + 04	2.29E + 06	0.39	1.02E + 01	21.2	21.0 – 21.5	n.d.	Cataract Creek
c		*2.44E + 06*	*4.21E + 06*	*−0.69*	*6.00E – 06*	*145.4*	*139.1 – 151.7*	*n.d.*	

[a]Read 4.29E + 04 as 4.29×10^4.
[b]Channel location depicted on Figure 4a. Italics represent channel segments below knickpoints.
[c]Distance measured from Point Reyes Station (Figure 4).
[d]Calculated with $\theta_{ref} = 0.45$.
[e]Uncertainties (2σ) on normalized steepness index.

and 4); topographic characteristics of the basins are provided in Table 1. Geographic differences in watershed characteristics are significant and figure prominently in our eventual interpretation of the controls on topography in this landscape. In the sections that follow, we discuss the results of our analysis, focusing first on the spatial distribution of channel gradients along Bolinas Ridge. We then consider morphologic evidence from both channels and hillslopes for recent increases in incision rate within these watersheds. Finally, we examine the Cataract Creek/Lagunitas Creek watershed, east of the Bolinas Ridge (Figure 2) in an effort to more fully characterize the distribution of fluvial incision in the region north of Mount Tamalpais.

3.2. Channel Profiles Along Bolinas Ridge

[21] A majority of channels developed along the western flank of Bolinas Ridge exhibit smooth, concave-up profiles similar to those predicted by models of steady state channel

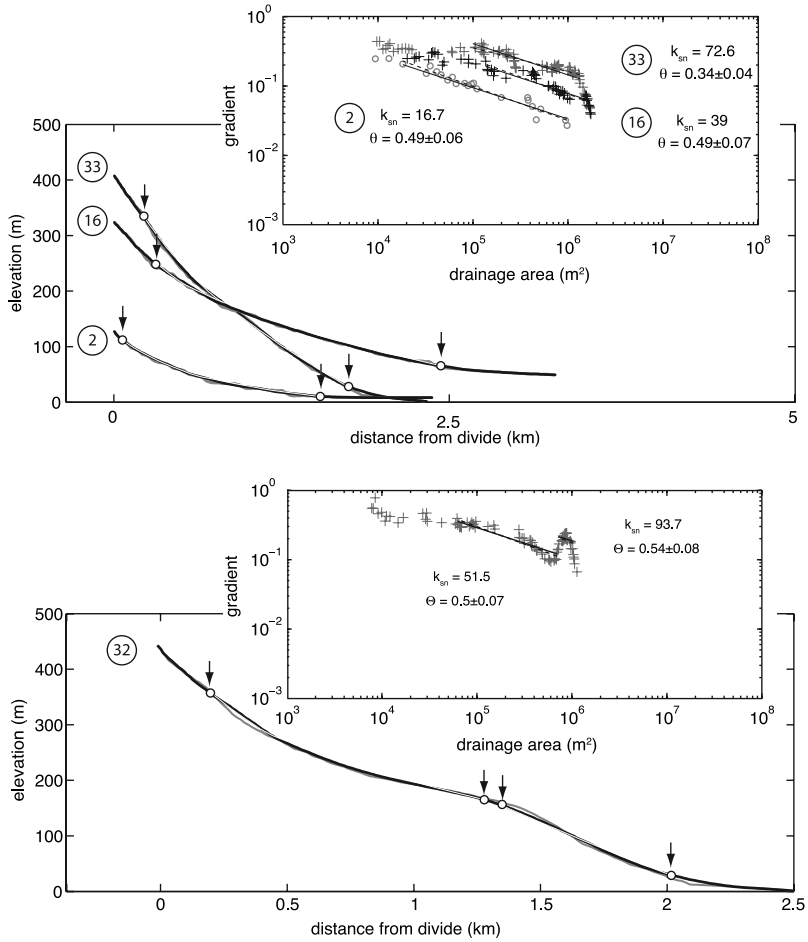

Figure 3. Representative channel profiles from Bolinas Ridge. Insets show slope-area data which are used to characterize channel concavity and steepness (see text for details). (top) Comparison of channel profile steepness from the north (channel 2), central (channel 16), and south (channel 33) portions of the Bolinas Ridge. Gradient-drainage area data (inset) show that channels are progressively steeper in the south with similar concavities. Channel numbers refer to designation on Table 1. Dashed lines are raw regression of gradient-area data, and solid lines are regression with reference concavity (θ_{ref}) used to determine the normalized steepness index (k_{sn}). Gray lines on longitudinal profiles represent the raw (unsmoothed) elevation data, black lines show the smoothed data, and white lines show the profile predicted by the regression. Regression interval is shown by arrows. (bottom) Example of a transient profile (channel 32, Table 1) characterized by a distinct convexity midway along the channel profile and high gradients downstream (inset). Regression of individual channel segments above and below the knickpoint (marked by arrows) yield estimates of channel steepness index associated with each reach.

form [e.g., *Whipple and Tucker*, 1999]. Important exceptions occur, however, in approximately ¼ of the channels (Table 1), where distinct reaches of increased channel gradient occur in the lower portions of the channel, separated from more gentle upstream portions by convex knickpoints. Examples of each type of profile are shown in Figure 3, and the differences between channel types will be explored further below.

[22] Channels developed along Bolinas Ridge display a wide range of profile concavity indices (θ) that do not appear to exhibit any systematic variation along the ridge (Figure 4b). We exclude from this comparison reaches downstream of distinct convex knickpoints, as these represent disturbed stream segments with ubiquitously high values of θ (Table 1). Although the mean of all concavity indices ($\sim$0.66, Figure 4) is within the range of values typical for incising channels [*Whipple*, 2004], the degree of variability is pronounced, and a number of channels, particularly along the midsection of the transect (Figure 4), exhibit highly concave profiles.

[23] In contrast, normalized steepness indices (k_{sn}) of these channels display a systematic increase from north to south along the ridge. At the north end of the transect, k_{sn} values are relatively uniform (15–20), reflecting low-gradient streams (Figure 3, top). Between 5 and 10 km south along the transect, however, k_{sn} values begin to increase and reach a maximum value of $\sim$120 near the junction between Bolinas Ridge and the Mount Tamalpais massif (Figure 4). Beyond this point to the south, k_{sn} values decrease sharply. Importantly, this spatial pattern in channel

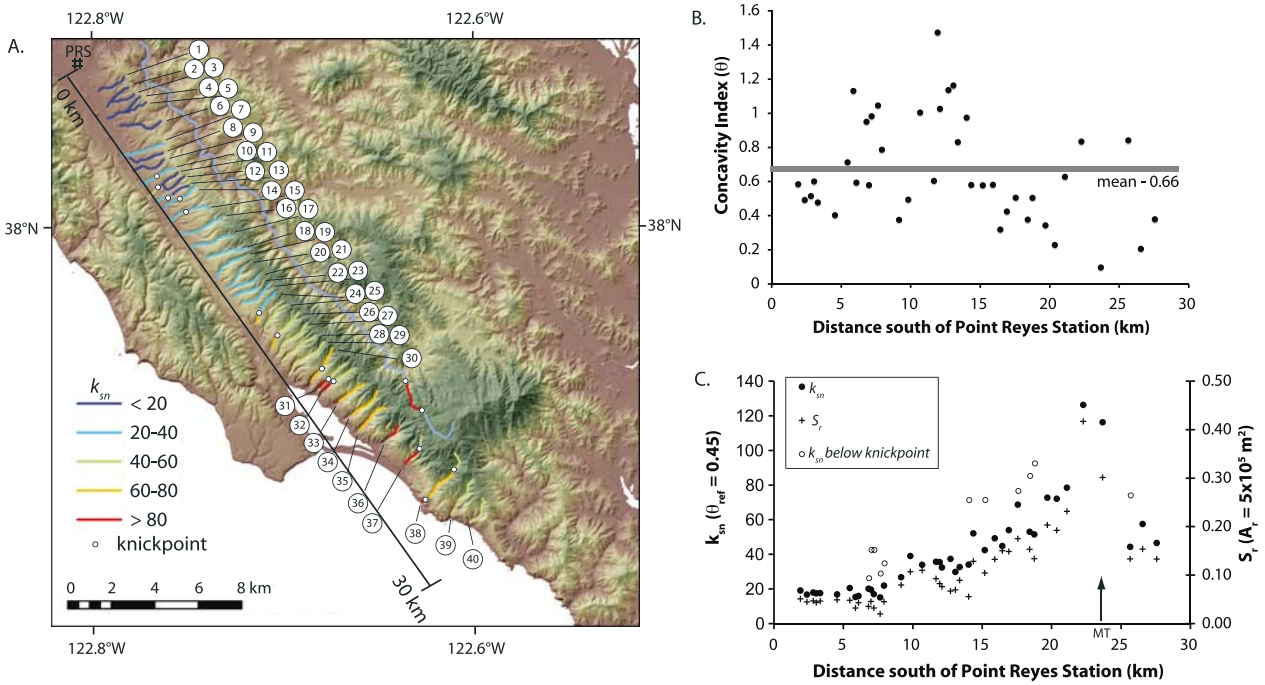

Figure 4. Topographic characteristic of channels in the Bolinas Ridge region. (a) Map of the distribution of normalized channel steepness (k_{sn}). White circles represent knickpoints in channel profiles marking abrupt change in k_{sn}. Cross-section line represents the reference scale for graphs at right, and numbers refer to the channel data in Table 1. (b) Channel concavity (θ) as a function of distance along Bolinas Ridge (south of Point Reyes Station; see Figure 4a for location). (c) Channel steepness (k_{sn}) as a function of distance. Note that reference concavity ($\theta_{ref} = 0.45$) is chosen for direct comparison to other studies [e.g., *Wobus et al.*, 2006b] and does not impact the spatial pattern. Open circles represent channel segments above knickpoints, and solid circles represent downstream segments. Crosses represent reference slope measurements [*Sklar and Dietrich*, 1998]. Both measures of channel gradient normalized for differences in drainage area record a distinct increase from north to south along the ridge. MT, location of Mount Tamalpais.

gradient is independent of the presence of knickpoints in the channels. Channel reaches downstream of knickpoints (open circles on Figure 4c) are systematically steeper than upstream reaches in a given channel (solid circles in Figure 4c), but both record a progressive steepening toward the south.

[24] The spatial pattern we observe in channel steepness indices (k_{sn}) is not a consequence of our choice of the upstream bound on the regression interval. Although systematic inclusion of data from the colluvial/hillslope regime in more southerly channels could impart a bias to the spatial pattern of k_{sn} values, we were conservative in our choice of regression intervals to capture only the downstream, fluvial scaling regime (see Table 1 for data). We recognize that in many cases, the transition in scaling regimes appears to occur over a range of drainage areas [*Stock and Dietrich*, 2003], rendering choice of regression open to a degree of interpretation. For example, in Figure 3, one might argue that the middle regression (black crosses, Figure 3, top, inset) could extend up to drainage areas $\sim 8 \times 10^4$ m^2. However, this would not change the regression parameters significantly, as the trend from the fluvial scaling encompasses these data. Thus we do not place great significance in the exact location of this transition, as determined from the available elevation data. Rather, we focus on the spatial differences in gradients along the entire fluvial scaling portion of the data. As exemplified again in Figure 3, channel gradients everywhere along the southern profile (Figure 3, top, inset) are greater than gradients along channels farther north. This leads us to conclude that our average k_{sn} values provide a reasonable measure of differences in channel steepness among profiles.

[25] We observe two clusters of knickpoints on channels along Bolinas Ridge. The first occurs between 7 and 8 km south along the transect, coincident with the initial increase in k_{sn} values (Figure 4). Lower reaches of these channels exhibit lower reaches that are approximately 1.5–2 times as steep as upstream reaches (Figure 3, bottom). The second cluster occurs between 15 and 20 km south along the transect, and downstream reaches show a similar relative increase in k_{sn} (Figure 4). Although not expressed in every channel, the systematic association of knickpoint position along the transect and the similarity of the relative difference in channel steepness across the knickpoints both suggest that the presence of knickpoints in these channels reflects active incision and transient adjustment of channel gradients. Knickpoints do not appear to be static features in this landscape.

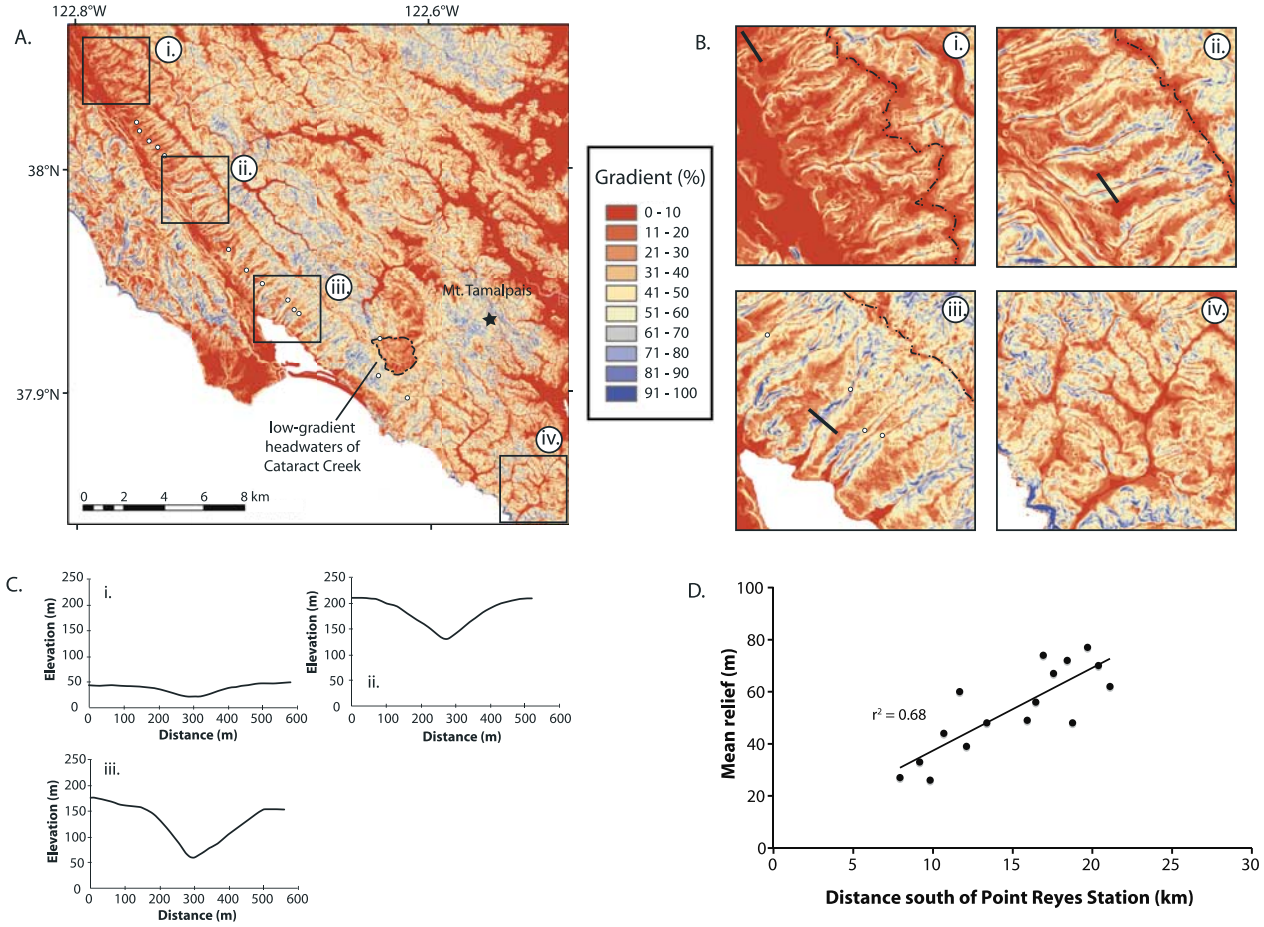

Figure 5. Hillslope gradients in the study area. (a) Gradient map derived from USGS 10 m DEM. Color map is chosen so that gradients >0.6 (~30°) are displayed in blue. White circles represent knickpoints along channel profiles. (b) Enlargements of watersheds along the west flank of Bolinas Ridge illustrate the prominence of threshold hillslopes along the lower reaches of channels. Dashed line highlights the ridge crest, and solid black lines represent cross sections in Figure 5c. Illustration iv is an enlargement of the Tennessee Valley region showing low-gradient alluvial valleys. (c) Topographic cross-valley profiles illustrating progressive change in hillslope gradient and relief. (d) Plot of the average relief on threshold hillslopes as a function of distance along Bolinas Ridge demonstrating that hillslopes grow progressively higher toward the south. This is interpreted to reflect a greater degree of recent channel incision (see text for details).

[26] Overall, we observe that k_{sn} values increase fourfold to sixfold from north to south along the Bolinas Ridge (Figure 4). The range of values depends largely on whether one considers the steepest two channels, directly west of the Mount Tamalpais massif, to be representative. Although these data are consistent with the overall trend of increasing k_{sn} values to the south, the abrupt increase in k_{sn} values may to some degree reflect scatter in the data. Thus we consider that the fourfold to sixfold range is a reasonable measure of the degree of uncertainty in the data. Estimates of channel gradient using the reference slope method [*Sklar and Dietrich*, 1998] yield a nearly identical pattern (crosses in Figure 4c). This result confirms our contention that spatial patterns in k_{sn} are not an artifact of measurement technique and is consistent with previous studies indicating that both methods provide an equivalent measure of normalized channel gradients [e.g., *Kirby et al.*, 2003].

3.3. Hillslope Gradients and Evidence for Transient Incision

[27] Even a cursory examination of topography along Bolinas Ridge reveals significant differences in the character and ruggedness of the landscape along strike of the ridge. In the north, diffuse, rounded hillslopes give way to fairly gentle, low-gradient channels, whereas in the south, steep, dissected hillslopes drop precipitously into deep canyons (Figure 2). Although the DEM we used in this study is too coarse to allow detailed investigation of the curvature of hillslopes in the study area [e.g., *Roering et al.*, 1999], some first-order differences are apparent in the distribution of hillslope gradients along Bolinas Ridge.

[28] At the north end of the ridge, near the town of Point Reyes Station, hillslopes display broad, low-gradient interfluves that steepen as they approach the channels. Hillslope gradients remain fairly moderate, however, only locally exceeding 0.4–0.5 (Figure 5a). Toward the south, however,

hillslope gradients along the valley sidewalls increase to >0.6 (~30°), defining a steep "inner gorge". Although these features are intermittently developed along any single channel, they appear to be nearly ubiquitous features of watersheds along the central and southern portions of the Bolinas Ridge. The transition from low-gradient interfluves to threshold hillsides at the angle of repose is quite sharp in most catchments, and is often encompassed across 1–2 pixels in the DEM (10–20 m, Figure 5). In the field, high-gradient hillslopes are characterized by hummocky topography, thin soils, and evidence of recent shallow landslides.

[29] The degree to which these inner gorges are developed varies among channels. Although channels in the north typically have threshold hillslope gradients adjacent to the lower portions of the channel, those in the south extend along most of the fluvial network and merge with high-gradient hillslopes in the headwaters (Figure 5). Several gorges terminate midway up channels, coincident with prominent knickpoints in the channel profile (Figure 5b).

[30] In order to characterize the extent of inner gorge development, we measure the local relief developed on the inner gorge walls. We extract the difference in elevation between the channel bottom and the upper extent of hillslopes at or above gradients of 0.6 (~30°, inferred to be the upper extent of shallow landslides). We then take the average value of this measure along the channel as representative of the mean relief on the inner gorge. As shown in Figure 5d, however, the mean relief on the inner gorge walls increases systematically toward the south, suggesting that steeper channels are associated with a greater degree of relatively recent incision. In fact, the inner gorges become indistinct above the steepest channels, as threshold hillslopes extend nearly to the interfluves of these watersheds (Figure 5).

[31] An important contrast exists, however, with landscape form on the Marin Headlands, south of Mount Tamalpais (Figure 5b, illustration iv). Here, channels do not display a distinct inner gorge. Steep hillslopes are confined to cliffs near the coast and to lithologically resistant bedrock; we observe no systematic zone of high gradient adjacent to channels. In fact, most channels exhibit low-gradient, alluvial filled valleys [*Montgomery and Dietrich*, 1988]. This difference suggests that whatever process is responsible for driving incision along the flank of Bolinas Ridge, it is spatially restricted and has not impacted channels developed in the Marin Headlands.

[32] It is worth noting here that the presence of low-gradient interfluves along Bolinas Ridge has been previously recognized [*Anderson*, 1899; *Keenan*, 1976; *Lawson*, 1894]. *Keenan* [1976], in particular, conducted an extensive topographic and geologic study of "bench-like" landforms along the western slope of the ridge, and concluded that they did not reflect lithologic variations, deep-seated landslides, or subordinate strands of the San Andreas fault. The absence of marine deposits and the presence of thin (20–60 cm) soils led to the suggestion that these benches represented a formerly continuous, uplifted surface. Interestingly, this author's mapping suggests that the elevation of interfluves increases toward the south along a transect parallel to the Bolinas Ridge crest [*Keenan*, 1976].

[33] Overall, we interpret the presence of threshold hillslopes adjacent to channels as indicative of progressive steepening of convex, soil mantled hillslopes in response to recent incision along the channel network. Although threshold hillslopes have been argued to develop as a stable form in some landscapes [*Densmore et al.*, 1997], the systematic spatial differences in the relief on threshold hillslopes along Bolinas Ridge argues against this explanation. Moreover, although the difficulty of reconstructing hillslope relief prior to the onset of rapid incision precludes a quantitative estimate of the magnitude of incision along the channel network, differences in relief along the ridge suggest that channels in the south have experienced progressively greater total incision. Although we do not agree with *Keenan* [1976] that the interfluves were necessarily once continuous, our observations are consistent with a landscape that has experienced a recent increase in the rate of channel incision.

3.4. Cataract Creek Knickpoint

[34] In order to assess whether similar morphologic evidence for transient channel incision is present east of Bolinas Ridge, on the northern flank of the Mount Tamalpais massif (Figure 2), we examined channel gradients along the Cataract Creek/Lagunitas Creek watershed. Although the channel profile along the lower reaches of Lagunitas Creek is obscured by two reservoirs (Figure 6), the profile is generally characterized by relatively low gradients. Along the Cataract Creek tributary, however, we observe a prominent knickpoint that separates a steep ($k_{sn} \sim 145$) lower reach from a gentle, low-gradient ($k_{sn} \sim 21$) upper reach. The lower reach is characterized by a plane bed, bedrock-floored channel (Figure 6c) generally devoid of coarse sediment; relief on this channel segment reaches approximately 400 m. Large, blocky talus piles are present along portions of the reach and appear to reflect collapse of hillslope material into the channel. In contrast, the channel segment above the knickpoint is a fairly wide (3–5 m) and shallow channel that is mantled along its length by coarse, rounded bed material (Figure 6b).

[35] The knickpoint itself is a remarkably discrete feature; the transition in channel morphology and gradient occurs over <100 m of channel length. Moreover, it occurs entirely within a body of greenstone mapped east of Bolinas Ridge (Figure 2), and does not appear to be localized on a lithologic boundary. The whole of the Cataract Creek watershed above the knickpoint exhibits relatively gentle topographic gradients, in contrast to steep, threshold hillslopes that comprise much of the reach downstream (Figure 6). All of these observations again suggest that the knickpoint is not static, but rather separates two fundamentally different domains in the landscape: an upper landscape with channels and hillslopes that are adjusted to a previous rate of base level fall ("relict" landscape of *Crosby and Whipple* [2006]) and a lower landscape that is currently experiencing increased rates of channel incision.

4. Discussion

4.1. Spatial and Temporal Variations in Channel Incision

[36] The observation of systematic variations in channel steepness along the length of Bolinas Ridge in the absence of strong climatic gradients and/or variations in lithology is

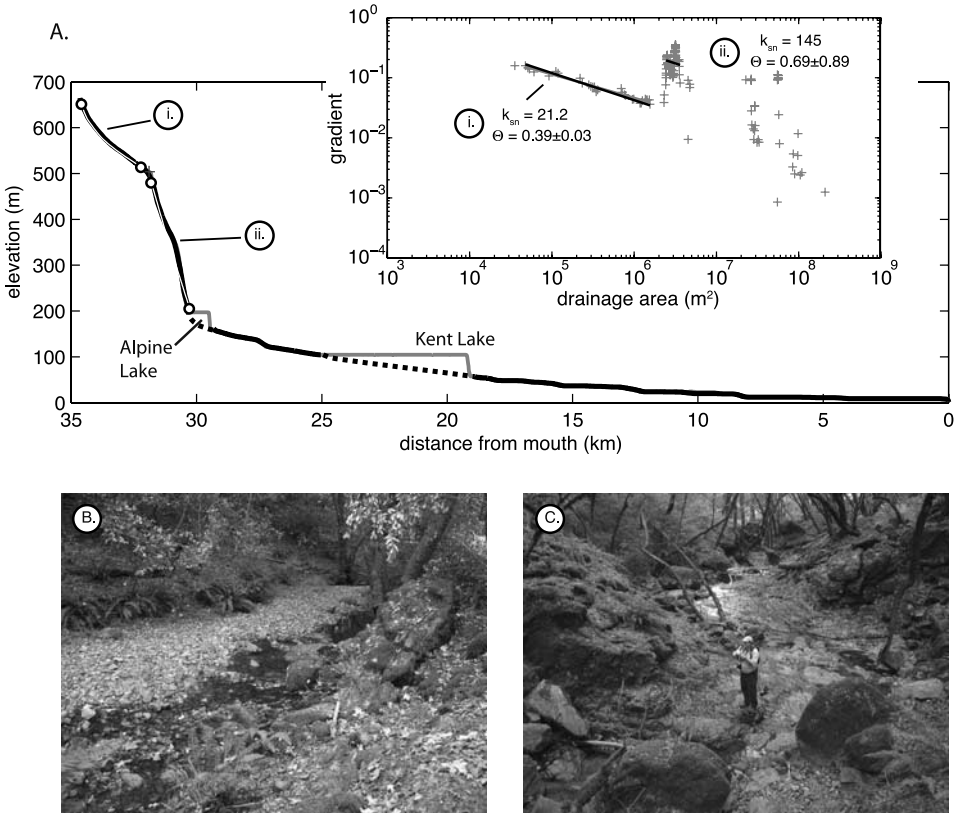

Figure 6. (a) Channel profile of Cataract Creek/Lagunitas Creek, east of Bolinas Ridge. The profile exhibits a steep reach just upstream of Alpine Lake (shaded lines represent the reservoir), on the northern flank of Mountain Tamalpais. Symbols and lines are as in Figure 3. Stream segments i and ii represent upstream and downstream portions of the Cataract Creek knickpoint, respectively. (b) Photograph of the sediment-mantled bed of Cataract Creek above the knickpoint. Channel is ~5 m wide. (c) Photograph of incised, plane bed bedrock channel downstream of knickpoint.

difficult to explain in the absence of differential rock uplift. Most theoretical models for fluvial incision into bedrock predict a positive monotonic relationship between channel gradients and incision rate [e.g., *Whipple*, 2004], a prediction borne out to some degree by empirical studies [*Kirby and Whipple*, 2001; *Lague and Davy*, 2003; *Snyder et al.*, 2000; *Wobus et al.*, 2006b]. This relationship is certainly modulated by thresholds for the inception of incision [*Snyder et al.*, 2003; *Tucker*, 2004] and by adjustments in channel width [*Duvall et al.*, 2004; *Finnegan et al.*, 2005]. However, neither of these effects is expected to generate an inverse correlation between k_{sn} and incision rate, and thus we suggest that the variation in observed k_{sn} reflects variations in incision rate along the ridge.

[37] Recent propositions for fluvial incision by bed load abrasion [*Sklar and Dietrich*, 1998, 2001, 2004] suggest that the highest transport stages may be less erosive than more moderate flows (a consequence of a decrease in the frequency of bed load impacts at high nondimensional shear stresses). This effect could, in principle, yield a nonmonotonic relationship between channel steepness (k_{sn}) and incision rate, as channels at high gradient become progressively less erosive. Such an effect has recently been suggested to be responsible for the formation of hanging fluvial valleys in Taiwan, where some tributaries are apparently unable to maintain connection to their trunk streams at high incision rate [*Wobus et al.*, 2006a]. Along Bolinas Ridge, however, the direct association of the steepest channels with the greatest relief on threshold hillslopes adjacent to those channels suggests that this effect is not responsible for the observed pattern of steepness values. Rather, steep channels appear to have been capable of maintaining high incision rates that have, in turn, driven an increase in hillslope gradients. Moreover, the association between the upstream extent of inner gorges with knickpoints in channels provides compelling evidence that channels are actively incising. Thus we contend that the observed pattern in channel steepness indices reflects spatial variations in erosion rate along the flank of Bolinas Ridge.

[38] The simplest explanation for such localized differences in channel incision is that they reflect differences in the rate of local rock uplift. Although we cannot uniquely deconvolve spatial from temporal variations in rock uplift (see tectonic implications, below), the fact that steepness indices of channel reaches upstream of knickpoints vary spatially suggests that the most recent pulse of incision (as recorded by threshold hillslopes and knickpoints) is not entirely responsible for the distribution of channel topography. Channels must have been steeper in the south prior to the most recent wave of incision, and thus we consider it likely that the primary signal is one of differential rock uplift increasing from north to south along the ridge.

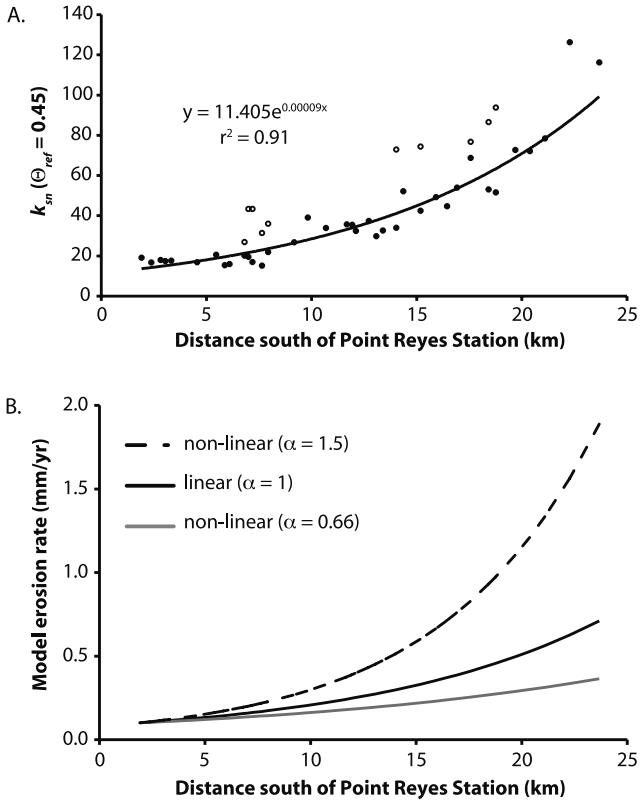

Figure 7. Predicted erosion rates along Bolinas Ridge. (a) Exponential fit to distribution of channel steepness. (b) Predicted erosion rates for various functional relationships between channel steepness (k_{sn}) and incision rate.

Importantly, a decrease in k_{sn} values at the southern end of our transect (Figure 4), and the apparent absence of recent incision along channels on the Marin Headlands, suggests that rock uplift rates decrease sharply to the south of Mount Tamalpais.

[39] The presence of inner gorges, some of which are associated with knickpoints, indicates a recent increase in the rate of incision along these systems, the origin of which remains somewhat enigmatic. Although the southern cluster of knickpoints occur on channels that debouch directly into the ocean and were likely impacted by glacioeustatic fluctuations in sea level, the northern cluster is relatively buffered from this influence by the long, transverse drainage (Olema Creek) parallel to the San Andreas fault. Moreover, well-developed inner gorges are present within portions of nearly all of the channels along the midsection of the ridge. All of these inner gorges terminate downstream at the intersection with the Olema valley, and do not continue along transverse drainage parallel to the San Andreas fault zone. The lack of continuity of the inner gorges with the coastline argues against a purely eustatic origin for these features.

[40] Rather, we suspect that the recent increase in incision likely reflects a relatively recent increase in the rates of differential rock uplift along the ridge. The absence of threshold hillslopes at the north end of the transect suggests that incision rates have remained slow enough such that soil transport by creep can keep pace with channel incision. In contrast, the absence of well-defined inner gorges at the southern end of the transect reflects the fact that threshold slopes extend nearly to interfluves. This observation is consistent with relatively high rates (and/or long durations) of incision in these drainages and suggests that these watersheds are approaching a steady state condition where hillslope relief becomes limited by threshold landslides [*Burbank et al.*, 1996].

4.2. Bounds on Erosion Rates

[41] Previous work characterizing hillslope erosion and soil production rates in Marin County allows us to place some first-order bounds on the rates of erosion along Bolinas Ridge and thus on the duration of transient channel incision. As noted above, studies of erosion rates using ^{10}Be in the Marin Headlands [*Heimsath et al.*, 1997, 1999] and on Point Reyes Peninsula [*Heimsath et al.*, 2005] suggest that convex hillslope noses are lowering at relatively slow rates (0.03–0.1 mm/yr) that depend largely on the thickness of overlying soil. Importantly, basin-wide erosion rates from these catchments yielded similar rates to those on convex ridge crests (0.08–0.1 mm/yr). As both of these sample sites are outside of the region of active incision on the flank of Bolinas Ridge, and both are developed in different lithologies (Francisican mélange versus Salinian granite), we infer that the lower end of this range (0.03–0.05) is a reasonable, conservative approximation for the erosion rates along low-gradient channels and hillslopes at the north end of Bolinas Ridge.

[42] We approach the problem of extrapolating these rates by modeling functional relationships between channel steepness (k_{sn}) and incision rate drawn from previous studies. We fit an exponential curve to the distribution of steepness indices (Figure 7a). For those channels with knickpoints, we fit data from upstream channel reaches, but we note that the using the entire data set does not significantly impact the result. For simplicity, we represent the k_{sn}–erosion rate relationship with a model of the form $E = k_{sn}^{\alpha}$ where $0.66 < \alpha < 3$. Some workers have documented a linear correlation between incision rate and k_{sn} in fluvial systems [*Kirby and Whipple*, 2001; *Wobus et al.*, 2006b] and in debris flow/colluvial channels [*Lague and Davy*, 2003]. This simple model would predict that erosion rates vary by fourfold to sixfold along Bolinas Ridge, reaching a maximum value between 0.4 and 0.7 mm/yr adjacent to the Mount Tamalpais massif (Figure 7). Alternatively, if bedrock incision is linear with bed shear stress [e.g., *Howard and Kerby*, 1983], the functional relationship between k_{sn} and erosion rate becomes less than linear (a $\sim$ 0.66 [*Whipple and Tucker*, 1999]), suggesting that incision rate varies by a factor of only 3–4 along the ridge. We take this as a conservative estimate (Figure 7). Finally, studies of bedrock channels in coastal California, in contrast, have observed distinctly nonlinear relationships between k_{sn} and incision rate (a >1 [*Duvall et al.*, 2004; *Snyder et al.*, 2003]). For values of $\alpha < \sim$1.5, predicted incision rates could range as high as 1–2 mm/yr (Figure 7). We note that for greater values of α, the nonlinear increase in incision rate with observed k_{sn} values leads to unreasonably high incision rates (Figure 7). Further characterization of incision rates in these catchments thus has the potential to refine the relationship between k_{sn} and incision rate and

thus place constraints on the macroscopic response of channels to incision rate.

4.3. Implications for Transient Landscape Response

[43] Our results are consistent with conceptual models for hillslope response to increased rates of base level lowering at the channel/hillslope boundary that envision a transition to threshold gradients for landslides as incision rates outpace the rate of soil production [e.g., *Burbank et al.*, 1996; *Schmidt and Montgomery*, 1995]. Despite uncertainty in the magnitude of incision rate variations along Bolinas Ridge, the position of the first well-defined threshold hillslopes (Figure 6) is coincident with modeled channel incision rates of $\sim$0.1–0.2 mm/yr (linear model, Figure 7), values in excess of the maximum soil production rates inferred for this landscape [*Heimsath et al.*, 1997, 1999]. Although soil production rates have not been determined for the sandstones underlying Bolinas Ridge, the similarity between production rate functions determined from greywackes in the Marin Headlands [*Heimsath et al.*, 1997, 1999] and granites on Point Reyes Peninsula [*Heimsath et al.*, 2005] suggest that perhaps lithology plays a secondary role in this landscape. Thus the correspondence between our modeled channel incision rates and the first appearance of threshold hillslopes is consistent with the maximum soil production rates of *Heimsath et al.* [1997, 1999, 2005] and lends a degree of confidence to a linear relationship between channel steepness and incision rate. Notably, the sublinear model (α = 0.66) predicts that incision rates in excess of $\sim$0.1–0.2 mm/yr are not reached until significantly farther south along the profile (Figure 7). This observation perhaps indicates that this functional relationship between channel steepness and incision rate is not adequate to represent the distribution of incision in these channels. A fuller test of this hypothesis will require a more comprehensive investigation of erosion rates in this landscape.

[44] Response timescales of typical hillslopes in this landscape dominated by diffusive creep are fairly long (on the order 10^5 yr) [*Fernandes and Dietrich*, 1997]. A transition from soil creep to threshold processes (either landslides or nonlinear, disturbance-driven creep) could significantly reduce this time [e.g., *Roering et al.*, 2001]. If our models of channel incision rate are correct, the relief observed on threshold hillslopes could have easily developed during $\sim$200–400 kyr of channel incision. Given that threshold hillslopes have not propagated the entire distance to watershed divides, it seems straightforward to infer that complete landscape response to an increase in incision rate exceeds these timescales.

[45] Finally, our observations suggest that hillslopes are not the only limiting factor in landscape response. The association of channel knickpoints and threshold hillslopes in some channels provides a strong indication that the channels themselves have not fully responded to an increase in incision rate. Moreover, the presence of knickpoints in some but not all drainages suggests a rather complicated response of channel profiles to differential rock uplift. The somewhat high and variable concavity of channels without knickpoints is consistent with the transient response of transport-limited channels [*Whipple and Tucker*, 2002]. If the channels are primarily transport-limited, and hillslope sediment flux has not yet fully adjusted to the rate of incision, channel gradients are likely still in a dynamic phase of adjustment. Testing these hypotheses will require a more comprehensive understanding of the distribution of erosion rates along Bolinas Ridge.

4.4. Tectonic Implications

[46] Regardless of the absolute magnitude of incision rates along the Bolinas Ridge, the spatial pattern is difficult to explain by any means other than differential rock uplift. Variations in channel profile form are not correlated with differences in lithology nor in climate. Moreover, as argued above, apparent differences in the rate of channel incision inferred from valley cross-sectional form indicates that spatial differences in channel steepness reflect a dynamic adjustment to spatially variable forcing and do not simply represent a static, relict form.

[47] Several independent possibilities exist to explain the inferred spatial pattern of incision rate variations. In the first case, the Bolinas Ridge region may represent a growing fold whose axis is subparallel to the San Andreas fault, analogous to numerous structures in the Carrizo Plain section of the fault in central California (e.g., Coalinga anticline). In this scenario, along-strike differences in channel profile form would reflect a propagating fold, such that low-gradient channels at the north and south ends of the ridge have just begun to experience increased rates of rock uplift, while those near the center have been experiencing high rates for a longer period of time. Such a model would be consistent with a transpressional component of deformation across the San Andreas. Geodetic data in the San Francisco Bay area have been used to argue both for [*Argus and Gordon*, 2001; *Murray and Segall*, 2001; *Prescott et al.*, 2001] and against [*d'Alessio et al.*, 2005; *Savage et al.*, 1998, 2004] contraction across the Coast Ranges. Although these data may not, at present, be able to resolve whether differential rock uplift along Bolinas Ridge reflects contraction across the San Andreas, it is notable that even those studies claiming to resolve fault-normal contraction [e.g., *Argus and Gordon*, 2001; *Murray and Segall*, 2001; *Prescott et al.*, 2001] consider shortening to be localized along the eastern margin of the Coast Ranges, consistent with geologic data [*Unruh and Lettis*, 1998]. Thus regional transpression across Marin County seems to us an unlikely mechanism to produce the inferred pattern of differential rock uplift along Bolinas Ridge.

[48] A second possibility may be that deformation in the Mount Tamalpais region is associated with the intersection of the San Gregorio and San Andreas faults. The San Gregorio fault is interpreted to link with the San Andreas just offshore of the Marin peninsula, providing an explanation for different rates of slip on the San Andreas north and south of the San Francisco Bay [*Working Group on California Earthquake Probabilities*, 2003]. We consider it unlikely that the tip of the San Gregorio fault exerts a strong influence across the San Andreas for the following reasons. First, seismic data indicate that Salinian basement is thrust over the margin of the Pacific plate [*Page and Brocher*, 1993] and that the San Gregorio fault is likely confined to the overthrust wedge. Relative motion across the fault thus need not generate deformation east of the San Andreas. Rather, the junction of the fault systems could be free to migrate northward with continued slip on the San

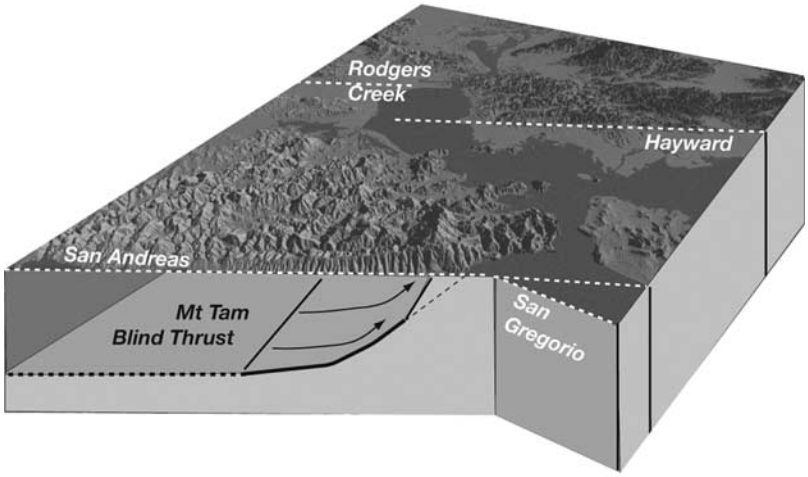

Figure 8. Cartoon of potential geometry of blind fault consistent with distribution of channel gradients. Surface is a perspective image of topography in the region. Dashed lines are faults.

Andreas. Second, if differential rock uplift was a consequence of deformation at the fault intersection, one would expect a pattern of rock uplift that decays toward the south, as the locus of deformation migrates northward. This model is inconsistent with the asymmetry of differential rock uplift we infer from our analysis.

[49] In the third scenario, the spatial pattern of channel incision reflects a quasi-stationary pattern of rock uplift developed above a blind fault oriented at a high angle to the San Andreas fault. We note that the asymmetry of the distribution of k_{sn} values along the Bolinas Ridge (Figure 4) bears a strong resemblance to the pattern of deformation expected above a blind thrust [*Ellis and Densmore*, 2006; *Lavé and Avouac*, 2000; *Molnar*, 1987]. In this model, the San Andreas acts as a free boundary, such that spatial variations in erosion rate provide a cross-sectional view of the pattern of rock uplift.

[50] Several lines of evidence suggest that a portion of Marin County east of the San Andreas may be experiencing similar patterns of differential rock uplift. First, the topography east of Bolinas Ridge also generally increases toward the south, mimicking the increase along the crest of the ridge (Figure 1b). Active incision along the northern flank of Mount Tamalpais in the Cataract Creek drainage appears to be coincident with the region of high channel gradients (and inferred incision rate) on the west side of Bolinas Ridge (Figure 4a). Moreover, the low-gradient portions of the Cataract Creek watershed above the knickpoint (Figure 5) define a broad, low-relief upland with a general dip to the north, consistent with the asymmetric decrease in channel steepness observed along Bolinas Ridge. Finally, the sharp change in relief across the steep southern flank of Mount Tamalpais itself, absent mapped differences in lithology [*Blake et al.*, 2000], mimics the decrease in steepness indices at the southern end of our transect. All of these observations suggest that northwest-southeast gradients in rock uplift extend at least to the northeastern flank of Mount Tamalpais, 10–15 km east of the San Andreas fault (Figure 4). Thus we consider that variations in landscape form are best explained by deformation above a blind thrust, dipping to the north, and with a buried fault tip somewhere in the vicinity of Mount Tamalpais (Figure 8).

[51] The eastward extent of such a structure, however, remains uncertain. Beyond the topographic edifice of Mount Tamalpais, low-gradient alluvial valleys drain south, through the eastern portion of Marin County with little apparent disruption (Figure 4). The absence of recent incision on these systems seems to preclude the presence of a structure with significant slip trending east from Mount Tamalpais. High topography does exist to the north of Mount Tamalpais (Figure 2), and may reflect a continuation of deformation northward. We caution, however, that this remains speculative, and that lithologic variations within the Franciscan terrane may be responsible for differences in topographic relief. Thus, although we have compelling evidence for active deformation in the Mount Tamalpais/Bolinas Ridge region, the eastward extent of differential rock uplift remains uncertain. Work is currently in progress to test the sensitivity of the surface deformation field to variations in fault geometry, extent, and slip rate of this potential structure [*Johnson et al.*, 2007].

[52] We note here, however, that even the most conservative estimates of erosion rate variation with channel steepness (Figure 7) predict erosion rates that vary by a factor of 3–5 of along Bolinas Ridge. These data are interpreted to provide a minimum bound on the rates of rock uplift along the ridge. If channel gradients are still in a transient state, and are not yet fully adjusted to the pattern of tectonic forcing, an inference that seems likely given the evidence for transient knickpoints and threshold hillslopes, actual variations in rock uplift rate could be greater. Thus our analysis suggests that we might expect rates of differential rock uplift along Bolinas Ridge to approach or exceed 0.5 mm/yr (Figure 7). These rates may, however, be a relatively young feature of the region. Apatite fission track data from the massif yield ages between 11 and 12 Ma, perhaps indicating a rapid cooling event around this time (T. A. Dumitru, written communication, 2006). These data require that rocks near the crest of Mount Tamalpais have resided at burial temperatures no greater than about 90°–100°C since ~10 Ma, indicative of limited exhumation

(probably less than a few km) since that time. Thus we infer that the rates and pattern of erosion implied by our results probably have been established for no more than 1–3 m.y. Our results provide an example of how geomorphic studies can help fill the temporal gap between decadal studies of crustal deformation and long-term rates inferred from thermochronologic methods.

5. Conclusions

[53] Our analysis of channel profiles in Marin County, California reveals the presence of systematic spatial patterns in channel steepness, within a monolithologic portion of the Franciscan terrane, that are interpreted to reflect spatial differences in incision rate east of the San Andreas fault. Differences in profile form are correlated to the development of threshold hillslopes that characterize valley walls, suggesting that increased rates of channel incision have driven a shift to hillslope erosion by mass transport processes. The transient morphology of the landscape thus provides confirmation that spatial patterns in channel steepness reflect a dynamic adjustment to spatially and temporally variable forcing. We argue that the observed pattern of channel response can only be explained by differential rock uplift along Bolinas Ridge, and is consistent with that expected above a blind thrust fault. Although rates of incision are not well-characterized in this landscape, a preliminary analysis of the relationship between channel steepness and incision rate suggests that differential rock uplift could exceed 0.5 mm/yr along the profile. Our analysis thus underscores the utility of geomorphic analysis as a reconnaissance tool to guide studies of active deformation in the upper crust while simultaneously highlighting the need for a better understanding of the quantitative relationship between channel incision process, rate and profile form.

References

Anderson, F. M. (1899), Geology of Point Reyes Peninsula, *Univ. Calif. Publ. Geol. Sci.*, *2*, 119–153.

Anderson, R. S. (1990), Evolution of the Northern Santa Cruz Mountains by advection of crust past a San Andreas fault bend, *Science*, *249*, 397–401.

Anderson, R. S., et al. (2006), Facing reality: Late Cenozoic evolution of smooth peaks, glacially ornamented valleys, and deep river gorges of Colorado's Front Range, in *Tectonics, Climate, and Landscape Evolution*, edited by S. D. Willett et al., *Spec. Pap. Geol. Soc. Am.*, *398*, 397–418.

Argus, D. F., and R. G. Gordon (2001), Present tectonic motion across the Coast Ranges and San Andreas fault system in central California, *Geol. Soc. Am. Bull.*, *113*, 1580–1592.

Atwater, T., and J. Stock (1998), Pacific–North America plate tectonics of the Neogene southwestern United States: An update, *Int. Geol. Rev.*, *40*, 375–402.

Bartow, J. A. (1991), The Cenozoic evolution of the San Joaquin Valley, California, *U.S. Geol. Surv. Prof. Pap.*, *1501*, 40 pp.

Blake, M. C., et al. (2000), Geologic map and map database of parts of Marin, San Francisco, Alameda, Contra Costa, and Sonoma Counties, California.

Burbank, D. W., et al. (1996), Bedrock incision, rock uplift and threshold hillslopes in the northwestern Himalayas, *Nature*, *379*, 505–510.

Cowie, P. A., and G. P. Roberts (2001), Constraining slip rates and spacings for active normal faults, *J. Struct. Geol.*, *23*, 1901–1915.

Crosby, B. T., and K. X. Whipple (2006), Knickpoint initiation and distribution within fluvial networks: 236 waterfalls in the Waipaoa River, North Island, New Zealand, *Geomorphology*, *82*, 16–38.

d'Alessio, M. A., I. A. Johanson, R. Bürgmann, D. A. Schmidt, and M. H. Murray (2005), Slicing up the San Francisco Bay Area: Block kinematics and fault slip rates from GPS-derived surface velocities, *J. Geophys. Res.*, *110*, B06403, doi:10.1029/2004JB003496.

Densmore, A. L., et al. (1997), Hillslope evolution by bedrock landslides, *Science*, *275*, 369–372.

Dietrich, W. E., et al. (1992), Erosion thresholds and land surface morphology, *Geology*, *20*, 675–679.

Dietrich, W. E., et al. (1993), Analysis of erosion thresholds, channel networks, and landscape morphology using a digital terrain model, *J. Geol.*, *101*, 259–278.

Dietrich, W. E., D. G. Bellugi, L. S. Sklar, J. D. Stock, A. M. Heimsath, and J. J. Roering (2003), Geomorphic transport laws for predicting landscape form and dynamics, in *Prediction in Geomorphology*, *Geophys. Monogr. Ser.*, vol. 135, edited by P. R. Wilcock and R. M. Iverson, pp. 103–132, AGU, Washington, D. C.

Duvall, A., E. Kirby, and D. Burbank (2004), Tectonic and lithologic controls on bedrock channel profiles in coastal California, *J. Geophys. Res.*, *109*, F03002, doi:10.1029/2003JF000086.

Ellis, M. A., and A. L. Densmore (2006), First-order topography over blind thrusts, in *Tectonics, Climate, and Landscape Evolution*, edited by S. D. Willett et al., *Spec. Pap. Geol. Soc. of Am.*, *398*, 251–266.

Fernandes, N. F., and W. E. Dietrich (1997), Hillslope evolution by diffusive processes: The timescale for equilibrium adjustments, *Water Resour. Res.*, *33*, 1307–1318.

Finnegan, N. J., et al. (2005), Controls on the channel width of rivers: Implications for modeling of fluvial incision of bedrock, *Geology*, *33*, 229–232.

Flint, J. J. (1974), Stream gradient as a function of order, magnitude, and discharge, *Water Resour. Res.*, *10*, 969–973.

Furlong, K. P., and S. Y. Schwartz (2004), Influence of the Mendocino Triple Junction on the tectonics of coastal California, *Annu. Rev. Earth Planet. Sci.*, *32*, 403–433.

Furlong, K. P., et al. (2003), The Mendocino crustal conveyor: Making and breaking the California crust, *Int. Geol. Rev.*, *45*, 767–779.

Graham, S. A., et al. (1984), Basin evolution during change from convergent to transform continental-margin in central California, *AAPG Bull.*, *68*, 233–249.

Hack, J. T. (1973), Stream profile analysis and stream-gradient index, *J. Res. U.S. Geol. Surv.*, *1*, 421–429.

Hancock, G. S., et al. (1998), Beyond power: Bedrock river incision process and form, in *Rivers Over Rock: Fluvial Processes in Bedrock Channels*, *Geophys. Monogr. Ser.*, vol. 107, edited by K. J. Tinkler and E. E. Wohl, pp. 35–60, AGU, Washington, D. C.

Heimsath, A., et al. (1997), The soil production function and landscape equilibrium, *Nature*, *388*, 358–361.

Heimsath, A., et al. (1999), Cosmogenic nuclides, topography, and the spatial variation of soil depth, *Geomorphology*, *27*, 151–172.

Heimsath, A. M., et al. (2005), The illusion of diffusion: Field evidence for depth-dependent sediment transport, *Geology*, *33*, 949–952.

Hodges, K. V., et al. (2004), Quaternary deformation, river steepening, and heavy precipitation at the front of the Higher Himalayan ranges, *Earth Planet. Sci. Lett.*, *220*, 379–389.

Howard, A. D. (1994), A detachment-limited model of drainage basin evolution, *Water Resour. Res.*, *30*, 2261–2285.

Howard, A. D., and G. Kerby (1983), Channel changes in badlands, *Geol. Soc. Am. Bull.*, *94*, 739–752.

Howard, A. D., W. E. Dietrich, and M. A. Seidl (1994), Modeling fluvial erosion on regional to continental scales, *J. Geophys. Res.*, *99*, 13,971–13,986.

Hurtrez, J.-E., F. Lucazeau, J. Lavé, and J.-P. Avouac (1999), Investigation of the relationship between basin morphology, tectonic uplift, and denudation from the study of an active fold belt in the Siwalik Hills, central Nepal, *J. Geophys. Res.*, *104*, 12,779–12,796.

Jackson, M., S. Barrientos, R. Bilham, D. Kyestha, and B. Shrestha (1992), Uplift in the Nepal Himalaya revealed by spirit leveling, *Geophys. Res. Lett.*, *19*, 1539–1542.

Johnson, C., et al. (2007), Integrated geomorphic and geodynamic modeling of a potential blind thrust in the San Francisco Bay area, California, *Tectonophysics*, in press.

Jones, C. H., et al. (2004), Tectonics of Pliocene removal of lithosphere of the Sierra Nevada, California, *Geol. Soc. Am. Bull.*, *116*, 1408–1422.

Keenan, J. L. (1976), Distribution and origin of bench-like topography on Bolinas Ridge, California: A problem in geomorphology, M. A. thesis, 134 pp., San Francisco State Univ., San Francisco, Calif.

Kirby, E., and K. Whipple (2001), Quantifying differential rock-uplift rates via stream profile analysis, *Geology*, *29*, 415–418.

Kirby, E., K. X. Whipple, W. Tang, and Z. Chen (2003), Distribution of active rock uplift along the eastern margin of the Tibetan Plateau: Inferences from bedrock channel longitudinal profiles, *J. Geophys. Res.*, *108*(B4), 2217, doi:10.1029/2001JB000861.

Kobor, J. S., and J. J. Roering (2004), Systematic variation of bedrock channel gradients in the central Oregon Coast Range: Implications for rock uplift and shallow landsliding, *Geomorphology*, *62*, 239–256.

Lague, D., and P. Davy (2003), Constraints on the long-term colluvial erosion law by analyzing slope-area relationships at various tectonic up-

lift rates in the Siwalik Hills (Nepal), *J. Geophys. Res.*, *108*(B2), 2129, doi:10.1029/2002JB001893.
Lavé, J., and J. P. Avouac (2000), Active folding of fluvial terraces across the Siwalik Hills, Himalayas of central Nepal, *J. Geophys. Res.*, *105*, 5735–5770.
Lawson, A. C. (1894), The geomorphology of the coast of northern California, *Univ. Calif. Publ. Geol. Sci.*, *1*, 241–272.
Lettis, W. L., and J. Unruh (2000), Critical evaluation of the northern termination of the Calaveras fault, eastern San Francisco Bay, *Rep. 00-HQ-GR-0082*, Natl. Earthquake Hazard Reduct. Program, Gaithersburg, Md.
Moglen, G. E., and R. L. Bras (1995), The effect of spatial heterogeneities on geomorphic expression in a model of basin evolution, *Water Resour. Res.*, *31*, 2613–2623.
Molnar, P. (1987), Inversion of profiles of uplift rates for the geometry of dip-slip faults at depth, with examples from the Alps and Himalaya, *Ann. Geophys., Ser. B.*, *5*, 663–670.
Montgomery, D. R., and M. T. Brandon (2002), Topographic controls on erosion rates in tectonically active mountain ranges, *Earth Planet. Sci. Lett.*, *201*, 481–489.
Montgomery, D. R., and W. E. Dietrich (1988), Where do channels begin?, *Nature*, *336*, 232–234.
Montgomery, D. R., and W. E. Dietrich (1989), Source areas, drainage density, and channel initiation, *Water Resour. Res.*, *25*, 1907–1918.
Montgomery, D. R., and W. E. Dietrich (1992), Channel initiation and the problem of landscape scale, *Science*, *255*, 826–830.
Montgomery, D. R., and W. E. Dietrich (1994), A physically based model for the topographic control on shallow landsliding, *Water Resour. Res.*, *30*, 1153–1171.
Montgomery, D. R., and E. Foufoula-Georgiou (1993), Channel network source representation using digital elevation models, *Water Resour. Res.*, *29*, 1178–1191.
Murray, M. H., and P. Segall (2001), Modeling broadscale deformation in northern California and Nevada from plate motions and elastic strain accumulation, *Geophys. Res. Lett.*, *28*, 3215–4318.
Niemann, J. D., et al. (2001), A quantitative evaluation of Playfair's law and its use in testing long-term stream erosion models, *Earth Surf. Processes Landforms*, *26*, 1317–1332.
Page, B. M., and T. M. Brocher (1993), Thrusting of the central California margin over the edge of the Pacific plate during the transform regime, *Geology*, *21*, 635–638.
Page, B. M., et al. (1998), Late Cenozoic tectonics of the central and southern Coast Ranges of California, *Geol. Soc. Am. Bull.*, *110*, 846–876.
Prescott, W. H., J. C. Savage, J. L. Svarc, and D. Manaker (2001), Deformation across the Pacific–North America plate boundary near San Francisco, California, *J. Geophys. Res.*, *106*, 6673–6682.
Roe, G. H., et al. (2002), Effects of orographic precipitation variations on the concavity of steady-state river profiles, *Geology*, *30*, 143–146.
Roe, G. H., D. R. Montgomery, and B. Hallet (2003), Orographic precipitation and the relief of mountain ranges, *J. Geophys. Res.*, *108*(B6), 2315, doi:10.1029/2001JB001521.
Roering, J. J., J. W. Kirchner, and W. E. Dietrich (1999), Evidence for nonlinear, diffusive sediment transport on hillslopes and implications for landscape morphology, *Water Resour. Res.*, *35*, 853–870.
Roering, J. J., J. W. Kirchner, and W. E. Dietrich (2001), Hillslope evolution by nonlinear, slope-dependent transport: Steady state morphology and equilibrium adjustment timescales, *J. Geophys. Res.*, *106*, 16,499–16,513.
Rosenbloom, N. A., and R. S. Anderson (1994), Evolution of the marine terraced landscape, Santa Cruz, California, *J. Geophys. Res.*, *99*, 14,013–14,030.
Savage, J. C., R. W. Simpson, and M. H. Murray (1998), Strain accumulation rates in the San Francisco Bay area, 1972–1989, *J. Geophys. Res.*, *103*, 18,039–18,051.
Savage, J. C., W. Gan, W. H. Prescott, and J. L. Svarc (2004), Strain accumulation across the Coast Ranges at the latitude of San Francisco, 1994–2000, *J. Geophys. Res.*, *109*, B03413, doi:10.1029/2003JB002612.
Schmidt, K. M., and D. R. Montgomery (1995), Limits to relief, *Science*, *270*, 617–619.
Shaw, J. H., and J. Suppe (1996), Earthquake hazards of active blind-thrust faults under the central Los Angeles Basin, California, *J. Geophys. Res.*, *101*, 8623–8642.
Sklar, L., and W. E. Dietrich (1998), River longitudinal profiles and bedrock incision models: Stream power and the influence of sediment supply, in *Rivers Over Rock: Fluvial Processes in Bedrock Channels*, *Geophys. Monogr. Ser.*, vol. 107, edited by K. J. Tinkler and E. E. Wohl, pp. 237–260, AGU, Washington, D. C.
Sklar, L., and W. E. Dietrich (2001), Sediment and rock strength controls on river incision into bedrock, *Geology*, *29*, 1087–1090.
Sklar, L. S., and W. E. Dietrich (2004), A mechanistic model for river incision into bedrock by saltating bed load, *Water Resour. Res.*, *40*, W06301, doi:10.1029/2003WR002496.
Snyder, N. P., et al. (2000), Landscape response to tectonic forcing: Digital elevation model analysis of stream profiles in the Mendocino triple junction region, northern California, *Geol. Soc. Am. Bull.*, *112*, 1250–1263.
Snyder, N. P., K. X. Whipple, G. E. Tucker, and D. J. Merritts (2003), Importance of a stochastic distribution of floods and erosion thresholds in the bedrock river incision problem, *J. Geophys. Res.*, *108*(B2), 2117, doi:10.1029/2001JB001655.
Stein, R. S., and G. C. P. King (1984), Seismic potential revealed by surface folding: 1983 Coalinga, California, earthquake, *Science*, *224*, 869–872.
Stock, J., and W. E. Dietrich (2003), Valley incision by debris flows: Evidence of a topographic signature, *Water Resour. Res.*, *39*(4), 1089, doi:10.1029/2001WR001057.
Stock, J. D., and D. R. Montgomery (1999), Geologic constraints on bedrock river incision using the stream power law, *J. Geophys. Res.*, *104*, 4983–4993.
Tarboton, D. G., et al. (1989), Scaling and elevation in river networks, *Water Resour. Res.*, *25*, 2037–2051.
Tomkin, J. H., M. T. Brandon, F. J. Pazzaglia, J. R. Barbour, and S. D. Willett (2003), Quantitative testing of bedrock incision models for the Clearwater River, NW Washington State, *J. Geophys. Res.*, *108*(B6), 2308, doi:10.1029/2001JB000862.
Tucker, G. E. (2004), Drainage basin sensitivity to tectonic and climatic forcing: Implications of a stochastic model for the role of entrainment and erosion thresholds, *Earth Surf. Processes Landforms*, *29*, 185–205.
Tucker, G. E., and R. L. Bras (2000), A stochastic approach to modeling the role of rainfall variability in drainage basin evolution, *Water Resour. Res.*, *36*, 1953–1964.
Tucker, G. E., and R. L. Slingerland (1994), Erosional dynamics, flexural isostacy, and long-lived escarpments: A numerical modeling study, *J. Geophys. Res.*, *99*, 12,229–12,243.
Unruh, J. R., and W. R. Lettis (1998), Kinematics of transpressional deformation in the eastern San Francisco Bay region, California, *Geology*, *26*, 19–22.
van der Beek, P., and P. Bishop (2003), Cenozoic river profile development in the Upper Lachlan catchment (SE Australia) as a test of quantitative fluvial incision models, *J. Geophys. Res.*, *108*(B6), 2309, doi:10.1029/2002JB002125.
Whipple, K. X. (2001), Fluvial landscape response time: How plausible is steady-state denudation?, *Am. J. Sci.*, *301*, 313–325.
Whipple, K. X. (2004), Bedrock rivers and the geomorphology of active orogens, *Annu. Rev. Earth Planet. Science*, *32*, 151–185.
Whipple, K. X., and G. E. Tucker (1999), Dynamics of the stream-power river incision model: Implications for height limits of mountain ranges, landscape response timescales, and research needs, *J. Geophys. Res.*, *104*, 17,661–17,674.
Whipple, K. X., and G. E. Tucker (2002), Implications of sediment-flux-dependent river incision models for landscape evolution, *J. Geophys. Res.*, *107*(B2), 2039, doi:10.1029/2000JB000044.
Whipple, K. X., et al. (1999), Geomorphic limits to climate-induced increases in topographic relief, *Nature*, *401*, 39–43.
Whipple, K. X., et al. (2000), River incision into bedrock: Mechanics and relative efficacy of plucking, abrasion, and cavitation, *Geol. Soc. Am. Bull.*, *112*, 490–503.
Willgoose, G. (1994), A physical explanation for an observed-slope-elevation relationship for catchments with declining relief, *Water Resour. Res.*, *30*, 151–159.
Willgoose, G., R. L. Bras, and I. Rodriguez-Iturbe (1991), A coupled channel network growth and hillslope evolution model: 1. Theory, *Water Resour. Res.*, *27*, 1671–1684.
Wobus, C. W., et al. (2003), Has focused denudation sustained active thrusting at the Himalayan topographic front?, *Geology*, *31*, 861–864.
Wobus, C. W., B. T. Crosby, and K. X. Whipple (2006a), Hanging valleys in fluvial systems: Controls on occurrence and implications for landscape evolution, *J. Geophys. Res.*, *111*, F02017, doi:10.1029/2005JF000406.
Wobus, C. W., et al. (2006b), Tectonics from topography: Procedures, promise, and pitfalls, in *Tectonics, Climate, and Landscape Evolution*, edited by S. D. Willett et al., *Spec. Pap. Geol. Soc. Am.*, *398*, 55–74.
Working Group On California Earthquake Probabilities (2003), Earthquake probabilities in the San Francisco Bay region: 2002–2031, *U.S. Geol. Surv. Open File Rep.*, *03-214*, 10 pp.

K. Furlong, C. Johnson, and E. Kirby, Department of Geosciences, Pennsylvania State University, University Park, PA 16802, USA. (ekirby@geosc.psu.edu)
A. Heimsath, Department of Earth Science, Dartmouth College, Hanover, NH 03755, USA.